The Company of Biologists

TECHNIQUES AND RESOURCES

RESEARCH ARTICLE

Normal Table of *Xenopus* development: a new graphical resource

Natalya Zahn[1,*], Christina James-Zorn[2,*], Virgilio G. Ponferrada[2], Dany S. Adams[3], Julia Grzymkowski[4], Daniel R. Buchholz[5], Nanette M. Nascone-Yoder[4], Marko Horb[6], Sally A. Moody[7], Peter D. Vize[8] and Aaron M. Zorn[2,9,‡]

ABSTRACT

Normal tables of development are essential for studies of embryogenesis, serving as an important resource for model organisms, including the frog *Xenopus laevis*. *Xenopus* has long been used to study developmental and cell biology, and is an increasingly important model for human birth defects and disease, genomics, proteomics and toxicology. Scientists utilize Nieuwkoop and Faber's classic 'Normal Table of *Xenopus laevis* (Daudin)' and accompanying illustrations to enable experimental reproducibility and reuse the illustrations in new publications and teaching. However, it is no longer possible to obtain permission for these copyrighted illustrations. We present 133 new, high-quality illustrations of *X. laevis* development from fertilization to metamorphosis, with additional views that were not available in the original collection. All the images are available on Xenbase, the *Xenopus* knowledgebase (http://www.xenbase.org/entry/zahn.do), for download and reuse under an attributable, non-commercial creative commons license. Additionally, we have compiled a 'Landmarks Table' of key morphological features and marker gene expression that can be used to distinguish stages quickly and reliably (https://www.xenbase.org/entry/landmarks-table.do). This new open-access resource will facilitate *Xenopus* research and teaching in the decades to come.

KEY WORDS: *Xenopus laevis*, Normal table, Amphibian development, FETAX, EAMA, AMA, Metamorphosis, Embryo

INTRODUCTION

Normal tables of development are essential to allow different researchers to compare their results and to make experimental replication possible. Because the speed of *Xenopus* development depends upon the temperature of the water in which they grow, and these temperatures vary throughout the day and between individual laboratories, standardizing experiments to allow comparisons between laboratories and between experiments is inherently problematic. Since 1956, the standard reference for *Xenopus laevis* development has been the Normal Table of *Xenopus laevis* (Daudin) (hereafter referred to as the Normal Table), edited by Nieuwkoop and Faber (1956).

Chronicling the internal and external development of *Xenopus* 'from the fertilized egg till the end of metamorphosis', as the subtitle of the Nieuwkoop and Faber Normal Table states, started with field work to collect *X. laevis* from ponds near Stellenbosch in South Africa. The resulting work was an international collaboration of 28 embryologists, zoologists and field biologists, including the editors, from nine countries, all experts in the different organ systems in Anurans and other vertebrates. The primary data in the Normal Table was included in Chapter VI, expanded into 21 'divisions', which detailed the temporal development of organs and systems including the nervous systems and sense organs; the early axial system; the skeleton and musculature of head, trunk and tail; the lateral line, skin and pigmentation; brain; cephalic nerves; spine and spinal ganglia; eye; head; heart and vasculature; gonads, adrenal glands; and the intestinal tract. The last two divisions (XX and XXI) focused on the gross anatomical and histological changes in the alimentary system, such as intestinal gut coiling. Chapter VII then summarized all external and internal criteria in detail for each developmental stage in chronological order from Nieuwkoop and Faber (NF) stage 1 (fertilized egg) to NF stage 66 (the froglet) (Nieuwkoop and Faber, 1956, 1994). Internal development was elucidated by histological analysis, and although this data was extensively referenced, it was not included in the Normal Table (for a complete historical overview, see Hopwood, 2007). A later publication, an atlas of the histology of early *Xenopus* development by Hausen and Riebesell in 1991 addressed the need for an authoritative histological reference (Hausen and Riebesell, 1991).

Nieuwkoop and Faber based their staging system on discrete external morphology and internal features at a stable temperature, rather than hours post-fertilization or length of larvae, as had been done for earlier vertebrate normal tables. Thus, the NF staging system can be applied to many other *Xenopus* species, including *X. tropicalis*, a physically smaller species widely used in disease modeling owing to its simpler diploid genome (*X. laevis* is pseudotetraploid) (Khokha et al., 2002), and even the exceptionally large, dodecaploid *X. longipes*, an endangered species being reared in captivity in which tadpoles metamorphose at near full adult body size (Tapley et al., 2015). Although the length of tadpoles at each NF stage varies amongst species, the internal and external milestones, such as early cell divisions (NF stage 2-6), the beginning of gastrulation (NF stage 10), the beating of the heart (NF stage 33 and

[1]www.natalya.com, Cambridge, MA, USA. [2]Xenbase, Division of Developmental Biology, Cincinnati Children's Hospital Research Foundation, 3333 Burnet Ave, Cincinnati, OH 45229, USA. [3]Lucell Diagnostics Inc, 16 Stearns Street, Cambridge, MA 02138, USA. [4]Department of Molecular Biomedical Sciences, College of Veterinary Medicine, North Carolina State University, Raleigh, NC 27695, USA. [5]Department of Biology Sciences, University of Cincinnati, Cincinnati, OH 45221, USA. [6]National Xenopus Resource, Marine Biological Laboratory, Woods Hole, MA 02543, USA. [7]Department of Anatomy and Cell Biology, George Washington University Medical Center, Washington, DC 20037, USA. [8]Xenbase, Department of Biological Science, University of Calgary, Calgary, Alberta T2N 1N4, Canada. [9]Department of Pediatrics, University of Cincinnati College of Medicine, Cincinnati, OH 45229, USA.
*These authors contributed equally to this work

‡Author for correspondence (aaron.zorn@cchmc.org)

N.Z., 0000-0002-9982-3909; C.J., 0000-0001-5495-4588; V.G.P., 0000-0002-8590-7183; D.S.A., 0000-0003-2024-9746; J.G., 0000-0002-8465-0056; D.R.B., 0000-0002-9881-9924; N.M.N., 0000-0003-1301-5298; M.H., 0000-0002-5067-0518; S.A.M., 0000-0003-4192-1087; P.D.V., 0000-0001-8026-0424; A.M.Z., 0000-0003-3217-3590

DEVELOPMENT

34), gut coiling (NF stage 41-46) or limb development (NF stage 48-58) can be used to stage embryos in most *Xenopus* species.

One of the most frequently used parts of the Normal Table is the set of 125 drawings by J. J. Prijs. Created in the style of embryologists of the era, these were based on pencil drawings Job Faber made on his South African field trip. These illustrations were initially used to great advantage by the Nieuwkoop laboratory during the pre-genomic era to characterize the timing of inductive signaling involved in the formation of the mesoderm germ layer and the neural ectoderm (Nieuwkoop, 1973, 1985; Durston et al., 1989). Others quickly appreciated the advantages of precise staging to characterize when and where critical developmental events occurred, from germ layer induction to organ formation. From the start of molecular embryology in the 1990s, to the current single-cell genomic era, accurate developmental staging remains a crucial step in any experiment.

Now, more than 65 years after the original publication, J. J. Prijs' classic drawings are considered an essential resource and are used extensively in teaching and research. There has always been a demand to reuse these drawings in publications, yet it is no longer possible to obtain copyright permission. Nieuwkoop and Faber personally held copyright as editors, and this was reinstated in subsequent reprintings in 1967, 1975, and lastly in 1994. Xenbase was given permission to display the entire series NF drawings in 2008, and these can be downloaded for personal use; however, to the best of our knowledge, the Nieuwkoop and Faber images are not in the public domain and still require permission for subsequent reuse in publications. Herein lies the conundrum: it is no longer possible to obtain re-use permission as the copyright holders are both deceased, and the publisher of the latest edition, Garland Publishing, Inc. (New York and London), is out of business. There is literally no one from whom to request permission.

Aside from the copyright issues, a few limitations of the Normal Table drawings have become apparent over the years. A number of important views of embryos and tadpoles are missing from the collection. For example, there are no anterior views after NF stage 21, no ventral views of neurula or early tadpoles at NF stages 13-40, dorsal views from NF stages 28-59 are not included, and views of larger tadpoles and metamorphic stages are truncated, omitting the tail. In addition, the gut-coiling diagrams that accompanied NF stage 43-45 lack sufficient detail to reflect accurately stage-specific changes in digestive system development. To address these limitations, we generated a new, open-source graphical resource to be used in conjunction with the original Normal Table text. This new resource includes 133 new high-quality illustrations of *X. laevis* development, from the fertilized egg to metamorphosing tadpoles and froglets, adding to a set of 30 previously released Zahn drawings that focused on anterior views of craniofacial development from the XenHead project (Zahn et al., 2017). Importantly, the Zahn drawings have a total of 67 new views that were not in the original Normal Table, new gut-coiling diagrams and new images of metamorphic stages. Finally, we have compiled an extensive reference table that summarizes key morphological landmarks and gene expression markers that can be used to distinguish quickly and reliably one stage from the next for NF stages 1-66 (Table S1).

All the images in the Zahn series are available on Xenbase, the *Xenopus* knowledgebase (http://www.xenbase.org/entry/zahn.do), and can be downloaded and reused under an attributable, non-commercial creative commons license. This new open-access resource will enable *Xenopus* research and teaching in the decades to come.

RESOURCE DESCRIPTION
Planning the illustrations
We first compared the existing 125 Nieuwkoop and Faber illustrations, and the 30 Zahn drawings from the XenHead project (Zahn et al., 2017), to all potential views of *Xenopus* embryonic stages (NF stages 1-66) (Fig. S1). To define a scope of work we prioritized: (1) standard views (dorsal, lateral, ventral, anterior); (2) stages most frequently assessed in *Xenopus* research (based on curation of *Xenopus* literature in Xenbase); while (3) attempting to cover comprehensively development from fertilization to metamorphosis; and (4) adding additional views not included in the 1956 Normal Table, but deemed useful to current *Xenopus* research (e.g. anterior and ventral views). The result was a scope of work with 133 illustrations of 56 developmental stages, spanning fertilized egg to froglet stages, including a composite illustration of hindlimb and forelimb development and new gut-coiling diagrams. Of these drawings, 100 are fully rendered and shaded, and 33 are unshaded line drawings. In total, the Zahn collection now consists of 198 images of *X. laevis*, covering 60 of the 66 NF developmental stages, 73 more than the original 1956 artwork by J. J. Prijs (Fig. S1).

Xenopus laevis staging landmarks
Staging *Xenopus* embryos is a skill that takes considerable practice to master. Our concept for a series of 'staging landmarks' arose from students' comments highlighting the need for a simplified 'staging for beginners' chart. Our goal was to generate a list of external anatomical features that experienced bench scientists look for when staging embryos, which could be used by students at the bench and by newcomers to *Xenopus* development, in addition to seasoned experts. We liken the concept of *Xenopus* staging landmarks to 'birding field marks', a simple yet distinctive combination of just a few traits that birders use to identify morphologically similar bird species in the field (e.g. great egrets have a yellow bill and black feet, whereas snowy egrets have a black bill and yellow feet). With input from experienced *Xenopus* researchers, and with careful reference to descriptions from the 1994 edition of the Normal Table (Nieuwkoop and Faber, 1994), we distilled the 'external' morphological traits that distinguish each stage down to just a few key attributes that are visible under a stereomicroscope. Internal landmarks include major developmental processes and milestones from the Normal Table and findings from recent published research.

Leveraging decades of *in situ* hybridization (ISH) and immunohistochemistry (IHC) data curated in Xenbase, the Landmarks Table includes key gene expression markers of specific tissues and organs, data that was unknown at the time of the original Normal Table's publication, but which are now standard tools in most research laboratories. Importantly, molecular markers often indicate tissues and organ primordia prior to the overt formation of anatomical structures. For example, expression of the homeobox gene *nkx2-1* can be detected by ISH in the respiratory epithelium as early as NF stage 33-34, prior to the emergence of lung buds at NF stage 40 (Rankin et al., 2015).

The *Xenopus* staging Landmarks Table (Table S1) will be maintained on Xenbase (https://www.xenbase.org/entry/landmarks-table.do) as a living document, updated over time with community input and new research findings. Extensive gene expression data are also searchable on Xenbase using either the Expression Search tool (http://www.xenbase.org/geneExpression/geneExpressionSearch.do?method=display) or the *Xenopus* Anatomy Ontology (XAO)/Search Anatomy menu (http://www.xenbase.org/anatomy/anatomy.do?method=display&tabId=2).

DEVELOPMENT

Curated marker gene lists, based on published and community submitted gene expression images, are also provided for hundreds of XAO terms on Xenbase (James-Zorn et al., 2018).

Illustrations of *Xenopus laevis* development

NF stages 1-6: zygote and cleavage

Approximately 20 min after fertilization, the *Xenopus* egg, NF stage 1, rotates within the vitelline membrane such that the darkly pigmented animal hemisphere faces up and a lighter vegetal hemisphere faces down (Sive et al., 2007b). A condensation of dark pigment in the animal cortex indicates the sperm entry point, and a pale spot is often visible where the germinal vesicle has broken down (Fig. 1A). At room temperature (23°C), the first cell division occurs approximately 90 min post-fertilization, dividing the embryo into right and left halves. The fully cleaved two-cell embryo is NF stage 2 (Fig. 1B). The second cleavage ∼20-30 min later divides the embryo into dorsal and ventral halves to produce a four-cell embryo, NF stage 3 (Fig. 1C). During the next four cell cycles, the embryo continues to undergo synchronous, holoblastic cell division every 20-30 min at 23°C. The third cell division plane is perpendicular to the second, dividing the embryo into animal and vegetal halves resulting in an eight-cell embryo, NF stage 4 (Fig. 1D). Two subsequent cell divisions generate NF stage 5 (16-cell) (Fig. 1E) and NF stage 6 (32-cell) embryos with four rows of eight cells (Fig. 1F). Animal and lateral views of NF stage 3 to NF stage 6 embryos illustrate the often-noticeable difference between the lighter dorsal-animal blastomeres and the darker ventral-animal blastomeres. In addition, the animal hemisphere cells are noticeably smaller than cells in the vegetal hemispheres (Fig. 1D-F). Early molecular makers for NF stage 2 include *atp4a*, which marks the animal hemisphere; *vegt*, which marks the vegetal hemisphere and *nanos1*, which marks the germ plasm at NF stage 4 (Betley et al., 2002; Stennard et al., 1996; Walentek et al., 2012).

NF stages 6.5-12.5: blastula, gastrula and early neurula

Early *Xenopus* embryos undergo cell division without growing in size. By morula stage, NF stage 6.5 (Fig. 2A), cell division becomes asynchronous, being faster in the animal/dorsal than the vegetal/ventral region. At NF stage 7 (Fig. 2B), the fluid-filled blastopore cavity forms internally in the animal half of the embryo. It is no longer possible to count cell numbers reliably for NF stages 6.5-9, so the relative size of the darkly pigmented animal cells becomes the key feature distinguishing NF stage 8 (mid-blastula) (Fig. 2C) from NF stage 9 (late blastula) (Fig. 2D). This is an important staging watershed as early NF stage 8 marks the mid-blastula transition when, after 12 cell divisions, the cell cycle slows and large-scale zygotic transcription commences (Newport and Kirschner, 1982). At NF stage 7, *nodal5* is a molecular marker for the earliest evidence of zygotic transcription, and *gs17* and *nr1* are markers for the major initiation of zygotic transcription at NF stage 8. At late blastula stage, NF stage 9, *sox17* is a widely used marker for endoderm and *tbxt* (formerly known as *t* or *brachyury*) is the standard marker for mesoderm.

Gastrulation begins at NF stage 10 with the appearance of the blastopore lip in the vegetal dorsal region of the embryo (Fig. 2E). The invaginating dorsal blastopore lip becomes obvious as a darker indentation, caused by apical constriction of bottle cells and condensation of pigment (Moosmann et al., 2013). As gastrulation proceeds, the involuting marginal tissue at the blastopore lip extends laterally towards the ventral sides of the embryo, reaching almost halfway around the blastopore circumference at NF stage 10.5 (Fig. 2E). Between NF stages 11 and 12 (Fig. 2E,F) the vegetal cells
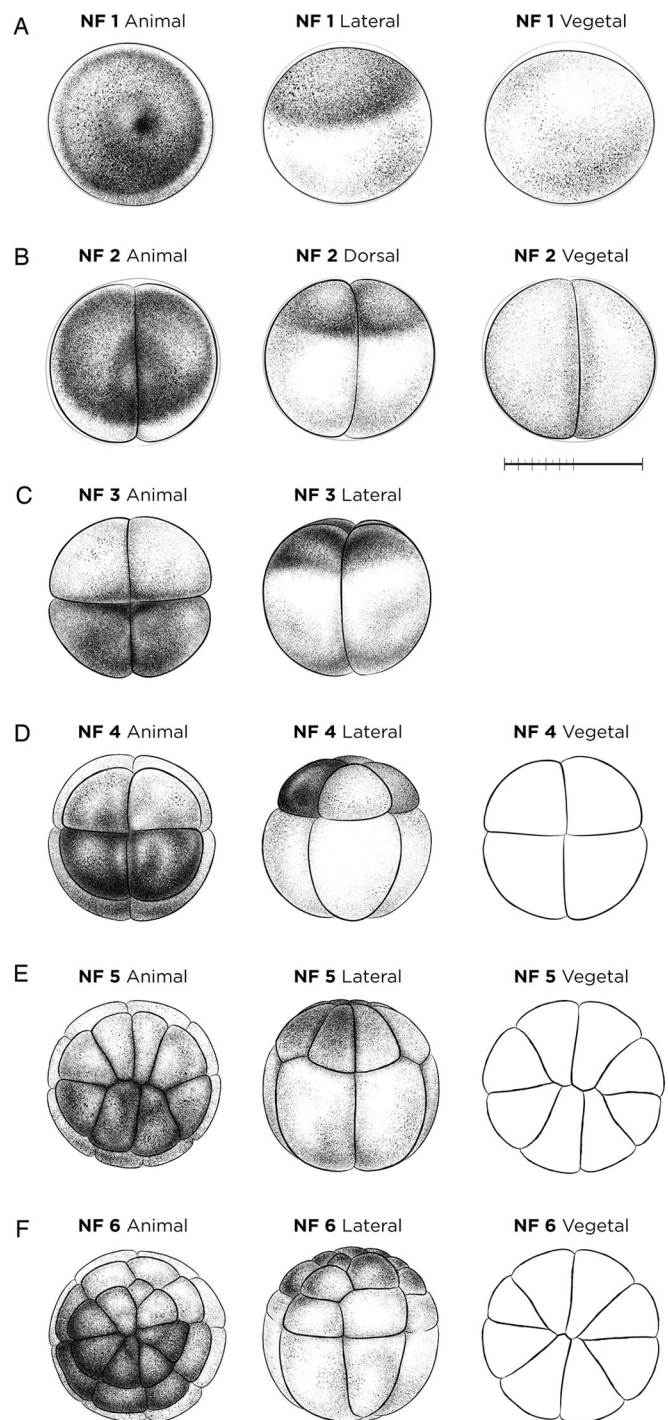

Fig. 1. Cleavage-stage *X. laevis* embryos. (A) The fertilized egg NF stage 1. (B) NF stage 2 (two-cell stage). (C) NF stage 3 (four-cell stage). (D) NF stage 4 (eight-cell stage). (E) NF stage 5 (16-cell stage). (F) NF stage 6 (32-cell stage). Vegetal/ventral views of NF stage 4-6 (D-F) are unshaded line drawings. See Table S1 for staging landmarks. Views as indicated. Scale bar: 1 mm.

are increasingly internalized, and the blastopore diameter progressively decreases, owing in large part to mediolateral intercalation of the underlying mesodermal cells (Keller and Sutherland, 2020). The relative dimensions of yolk plug to blastopore diameter, in combination with the extent of pigmentation along the blastopore lip, are key landmarks for stage
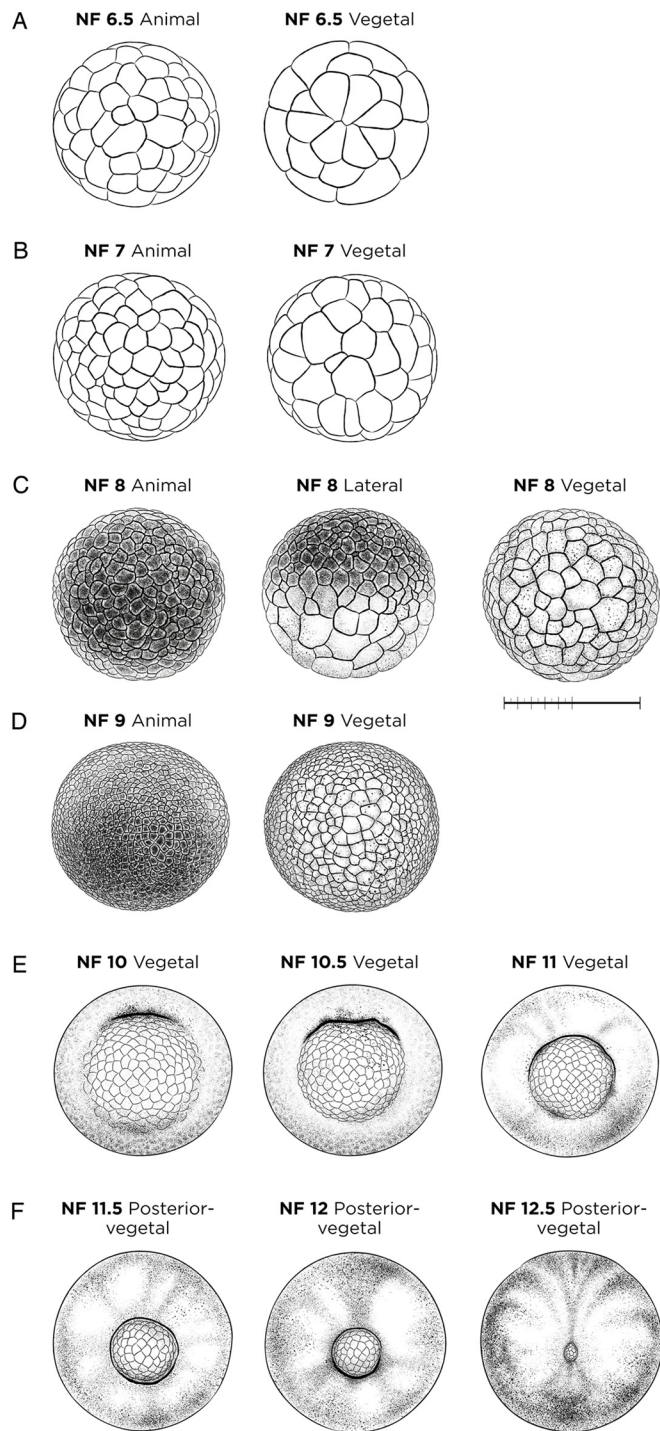
Fig. 2. Blastula-, gastrula- and early neurula-stage *X. laevis* embryos.
(A) NF stage 6.5 (morula); unshaded line drawing. (B) NF stage 7 (large-cell blastula); unshaded line drawing. (C) NF stage 8 (medium-cell blastula); membrane removed. (D) NF stage 9 (fine-cell blastula); membrane removed. (E) Gastrula-stage embryos, NF stage 10, NF stage 10.5 and NF stage 11; membrane removed. (F) NF stage 11.5, NF stage 12 and NF stage 12.5; membrane removed. See Table S1 for staging landmarks. Views as indicated. Scale bar: 1 mm.

determination during gastrulation (Fig. 2E,F). Based on molecular analysis, it is now clear that neural induction begins as early as NF stage 10.5 with *sox2* expression in the dorsal ectoderm (Gawantka et al., 1998). The neural plate is identifiable by NF stage 12 (Fig. 2F)

with a posterior constriction of the midline dorsal ectoderm, and by NF stage 12.5 (blastopore closed completely) (Fig. 2F) the notochord forms from mediolateral convergence of dorsal axial mesoderm under the neural ectoderm, a process identifiable by *chrd.1*, *nog* and *shh* expression (Roelink et al., 1994; Sasai, 1994; Fletcher and Harland, 2008).

NF stages 13-21: neurula
During neurulation, the neural plate deepens along the midline, and folds onto itself to form the neural tube (which later develops into the spinal cord and brain), a process which proceeds in a posterior to anterior direction. Accurate staging during early neurulation (Fig. 3A-E), NF stage 13 to NF stage 19 is very challenging as it is based on subtle differences in three traits: the three-dimensional shape of the neural folds, the width of the neural plate and the degree of neural tube closure. To visualize these features optimally, embryos are removed from the vitelline membrane (Sive et al., 2007a) so that the neural plate is not compressed. Internally, at NF stage 19 (Fig. 3E), the cranial neural crest forms at the border of the anterior neural plate and begins to migrate in 'streams' towards the ventral surface. A classic marker for early cranial neural crest streams is *sox9*, although many other genes also mark migrating neural crest cells (Spokony et al., 2002; Kuriyama and Mayor, 2008, 2009). NF stage 21 (Fig. 3F) is a popular stage to assay and staging is relatively easy, as the embryo is still curved dorsally, the neural tube is completely closed, and the developing eyes (optic vesicles) are visible as 'oblique oval spots' in lateral view and as slight bulges when viewed anteriorly. Molecular markers for NF stage 21 include *pax6* for the optic vesicle (Nakayama et al., 2015), *tekt3* and *foxj1* for multiciliated epidermal cells on the epidermis (Song et al., 2014; Chung et al., 2014), and *pax8* and *lim1* for the pronephric mesenchyme (Vize et al., 1995).

NF stages 22-28: tailbud stages
Anatomical landmarks for early tailbud embryos NF stages 22-26 (Fig. 4A-E) include the extent of dorsal curvature in the embryo, the number of pharyngeal 'bulges', the three-dimensionality and pigmentation of the developing eye, and the number/extent of anteriorly segregated, chevron-like somites. During this period, the somites, heart and pronephric kidney begin to form, while the embryo lengthens and becomes noticeably more slender. Although somite segmentation can be difficult to see under a light microscope until ~NF stages 27-28, molecular markers such as *myod1* can clarify the boundary between the formed somites and the presomitic mesoderm from NF stages 22 (Fig. 4A) onwards (Hopwood et al., 1992; Shang et al., 2020). NF stage 23 (Fig. 4B), referred to as a 'coffee bean' embryo, develops the inverted Y-shape, hatching gland on the anterior 'forehead', which expresses *cxcl14*, *astl3a.1* and *pax3* (Park et al., 2009). Key neurobehavioral milestones for tailbud stages include motor reactions to external stimuli at NF stage 24 and spontaneous movements at NF stage 26 (Fig. 4E), and at NF stage 28 (Fig. 4F) embryos that have been liberated from their vitelline membrane glide around a Petri dish as a result of the ciliary beating across the epidermis.

External landmarks for NF stage 28 (Fig. 4F) include a fully pigmented cement gland, the fin with an outer transparent and an inner translucent band that now extends to the cloaca, and a characteristic 'nose shape' to the extending tailbud. Internal landmarks for NF stage 28 include four distinct streams of *dlx2*-positive migrating cranial neural crest cells (Square et al., 2015), segregation of the epibranchial placodes, which express *neurog2*,
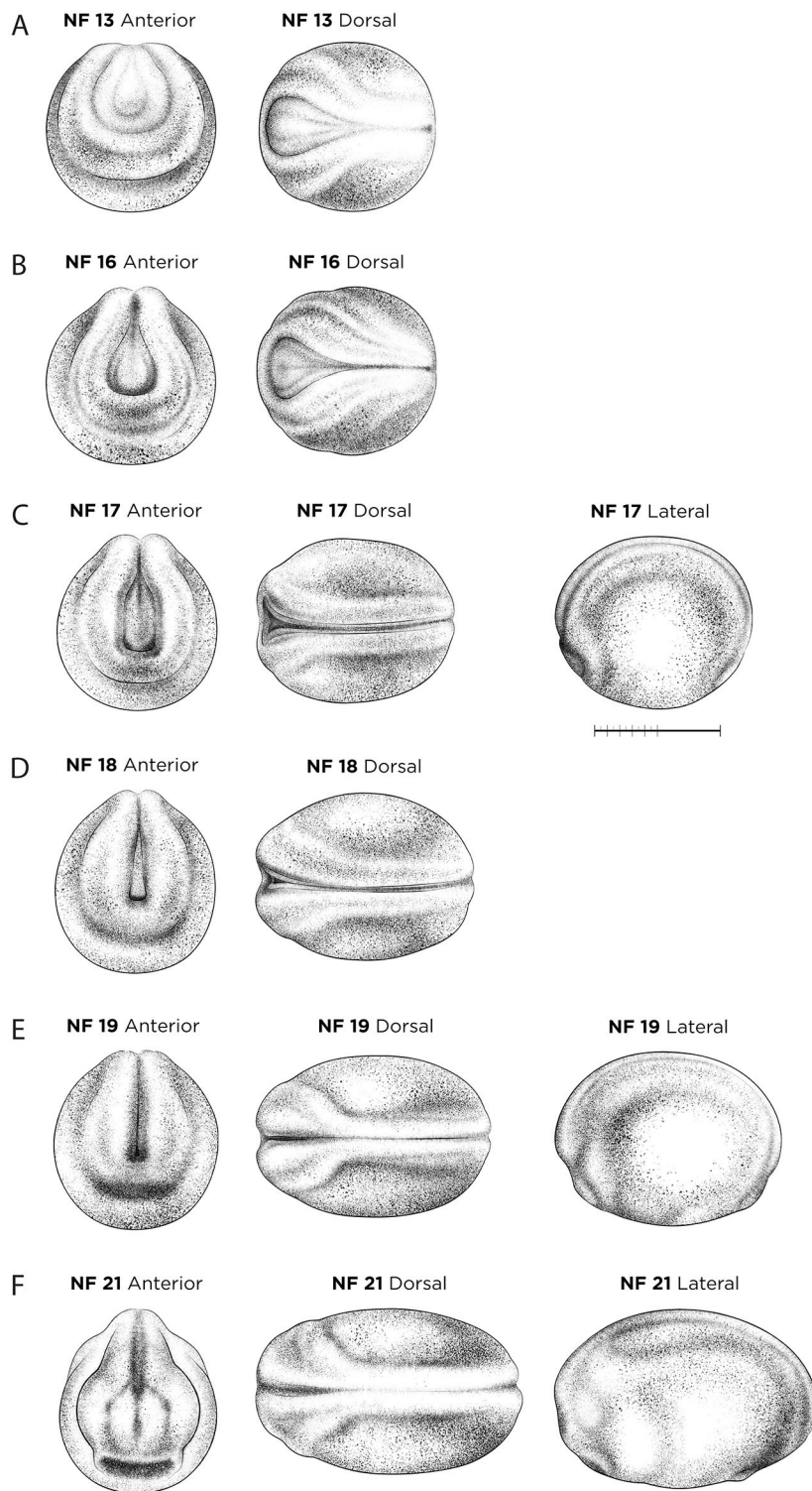
Fig. 3. Neural-stage *X. laevis* embryos. (A) NF stage 13 (slit-blastopore). (B) NF stage 16 (mid-neural fold). (C) NF stage 17 (late neural fold). (D) NF stage 18 (neural groove). (E) NF stage 19 (initial neural tube). (F) NF stage 21 (suture of neural groove completely closed). Orientation for anterior views is dorsal up; dorsal views have anterior left; lateral views have dorsal up and anterior left. See Table S1 for staging landmarks. Membrane removed in all embryos. Views as indicated. Scale bar: 1 mm.

foxi2 and *pax2* (Schlosser, 2006; Saint-Jeannet and Moody, 2014), and the first appearance of *pax2*- and *lhx1*-expressing nephrostomes (Vize et al., 1995; de Bakker et al., 2019). The heart of an NF stage 28 embryo has an endocardial tube surrounded by myocardium (marked by *tnni3*) and the beginning of the pericardial cavity. The otic vesicles (the auditory system primordia) detach from the epidermis at NF stage 28, yet are difficult to see under light microscopes, although they are commonly detected by *sox3*, *sox9* and *eya1* expression (Saint-Germain et al., 2004; Almasoudi and

Schlosser, 2021). Anteriorly, *fgf8* and *frzb1* mark the mouth primordium at NF stage 28 (Kennedy and Dickinson, 2012), and the complete formation of the hypochord (ventral to the notochord) can be seen by ISH for *vegfa* and *rspo3* (Cleaver et al., 1997; Kazanskaya et al., 2008).

NF stages 29-38: late tailbud and free-swimming tadpoles

Staging of late tailbud stages is best accomplished after removal of the vitelline membrane, focusing on eye morphology, tail and gut
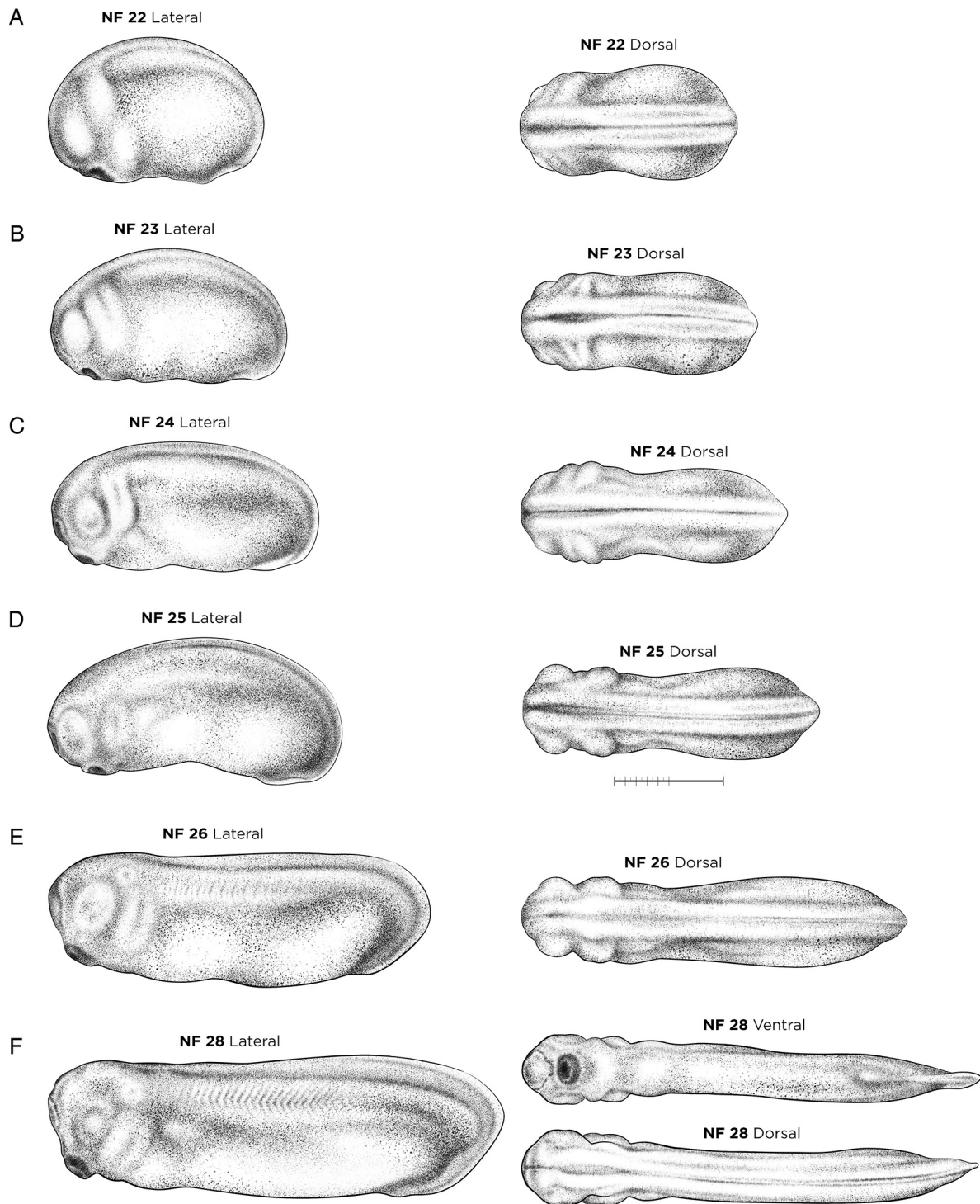
Fig. 4. Early tailbud-stage *X. laevis* embryos. (A) NF stage 22. (B) NF stage 23. (C) NF stage 24. (D) NF stage 25. (E) NF stage 26. (F) NF stage 28. Orientation for dorsal and ventral views is anterior left; lateral views have dorsal up and anterior left. See Table S1 for staging landmarks. Membrane removed in all embryos. Views as indicated. Scale bar: 1 mm.

development, and the spread of melanophores across the body (Table S1). The developing eye cup forms a gray disc at NF stage 29-30 (Fig. 5A) and its darkening color and degree of choroid fissure closure are easy to assess at NF stage 33-34 (darker above, still gray ventrally, open C-shape) (Fig. 5B), NF stage 35-36 (completely black, edges almost touching) (Fig. 5C) and NF stage 37-38 (fissure surfaces touching, but still slightly open) (Fig. 5D).

As embryos lengthen as a result of tail growth, their abdominal area simultaneously 'shortens' as undifferentiated gut endoderm begins to form distinct fore-, mid- and hindgut domains. The 'tail length to gut length' ratio is used as an external landmark (see Table S1), as is the angle formed between the tail and the posterior end of the gut (the future proctodeum) to distinguish NF stage 37-38 (140°), NF stage 39 (125°) and NF stage 40 (90°). Additional
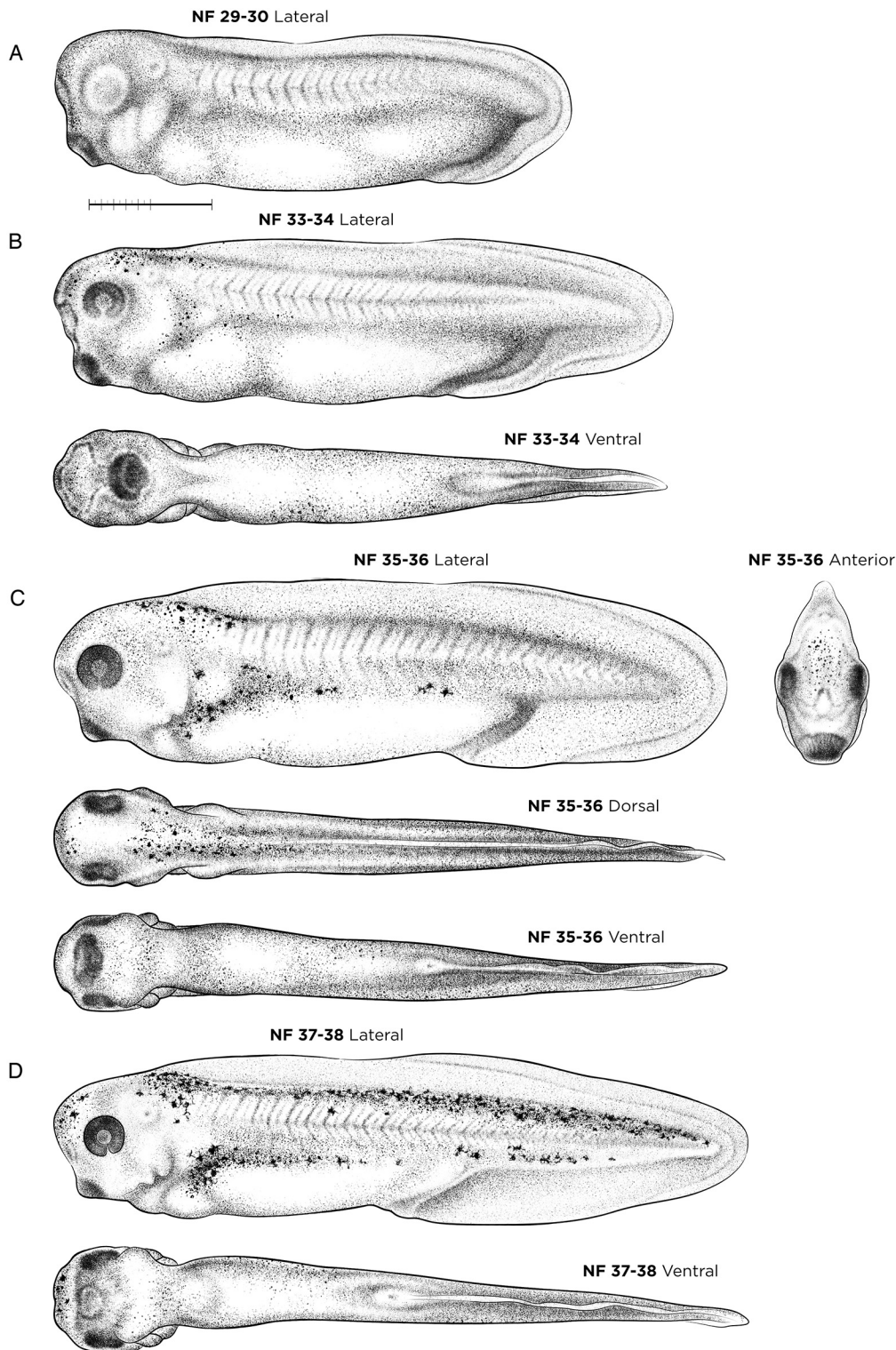
Fig. 5. Late tailbud-stage and free-swimming tadpole _X. laevis_ embryos. (A) NF stage 29-30. (B) NF stage 33-34. (C) NF stage 35-36. (D) NF stage 37-38. Orientation for dorsal and ventral views is anterior left; lateral views have dorsal up and anterior left. See Table S1 for staging landmarks. Membrane removed in all embryos. Views as indicated. Scale bar: 1 mm.

external landmarks include the extent of migration of the pigmented melanophores over the head and trunk starting at NF stage 33, and along the tail by NF stage 39. NF 35-36 marks a major behavioral transition as tadpoles naturally break free from their vitelline membrane to become free-swimming larvae/tadpoles.

A number of internal organogenesis milestones occur between NF stages 29 and 38 (Fig. 5). The embryonic heart forms as a linear tube with an anterior outflow tract, left ventricle, atrioventricular canal and atrium by NF stage 32. Heart looping and spontaneous heart contractions begin at NF stage 33-34 (Fig. 5B), with the heart obtaining a distinct S-shape with a separate atrium and ventricle by NF stage 35-36 (Fig. 5C). _Xenopus_ heart development can be visualized by ISH with the following markers: _hand2_, _tnni3_ and _actc1_ for the early heart (endocardial tube and cardiac mesoderm), and _aplnr_ for blood vessels (Drysdale et al., 1994; Parain et al., 2012; Vokes and Krieg, 2002). Between NF stage 32 and 35,

asymmetric expression of *pitx2* and *bmp4* is detected in the looping heart tube (Breckenridge et al., 2001). Blood flowing in the vasculature is visible by NF stage 37-38 (Fig. 5D), and *hba3* marks the ventral blood island (Kelley et al., 1994).

During this period, the bilateral pronephric kidney begins filtering the blood and osmoregulation. The glomus (where blood is filtered), nephrostomes (which collect the urine/filtrate) and pronephric duct (which drains the filtrate) form from the nephrogenic intermediate mesoderm by NF stage 28-30 (Beckers et al., 2021; Raciti et al., 2008; Zhou and Vize, 2004). The

pronephric duct fuses with the rectal diverticulum at NF stage 35-36, such that the entire pronephric kidney is functional by NF stage 37-38. The glomus expresses *wt1*, *nph1* and *cndp*, whereas the nephrostomes express *cfap161*, *pax2* and *lhx1* (Li et al., 2012; Beckers et al., 2021). Once epithelialized, the entire pronephric kidney and pronephric duct express *atp1a* and *slc4a4* along with various segment-specific solute transporters (Vize et al., 1995; de Bakker et al., 2019).

During NF stages 29-38 significant patterning also occurs in the central nervous tissue and digestive system. For example, *en2* (also
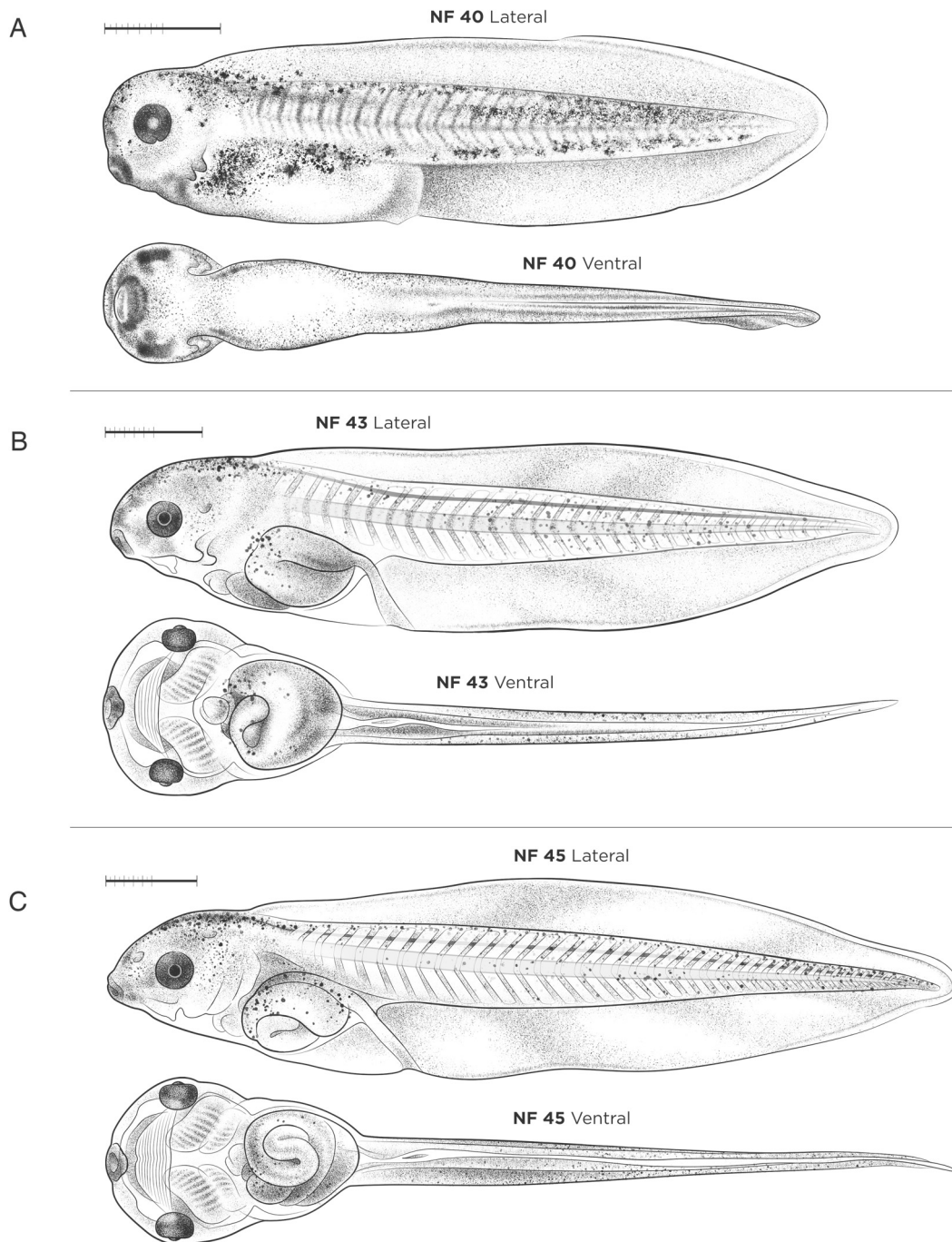

Fig. 6. Free-swimming and gut-coiling stages of *X. laevis* tadpoles. (A) NF stage 40. (B) NF stage 43. (C) NF stage 45. Orientation for ventral views is anterior left; lateral views have dorsal up and anterior left. See Table S1 for staging landmarks. Membrane removed in all embryos. Views as indicated. Scale bars: 1 mm.

known as *krox20*), *pax2* and *fgf8* mark the midbrain-hindbrain boundary (Brivanlou and Harland, 1989; Heller and Brändli, 1997; Lea et al., 2009), whereas *gsx1* identifies distinct regions of the forebrain (e.g. hypothalamus, zona limitans intrathalmica, medial ganglionic eminence and pretecum) and the hindbrain rhombomeres (r1-r5, r7 and r8) at NF stage 31-32 (Illes et al., 2009). In the gut tube, *hhex* marks the liver bud and *ptf1a* and *pdia2* the pancreatic buds (Pan et al., 2007; Zorn and Mason, 2001), whereas *nkx2-1* marks the thyroid gland and lung buds at NF stage 33-34 (Rankin et al., 2015).

NF stages 40-46: free-swimming tadpole

Morphogenesis of the digestive and respiratory systems are the major milestones occurring during the late free-swimming tadpole

and pre-metamorphosis stages (Figs 6A-C and 7). Many of these events can be readily observed as the body wall of tadpoles becomes more transparent. The foregut gives rise to the esophagus, trachea, lungs, stomach, duodenum, liver, pancreas and gall bladder, whereas the midgut and hindgut give rise to the intestine and cloaca, respectively. At NF stage 40 (Fig. 6A), external landmarks include the completely closed choroidal fissure and clearly visible blood circulating through the gills. NF stage 40 tadpoles will take gulps air from the surface at this stage, although their lungs are not yet functional. Internally, the liver and pancreatic organ buds are obvious at NF stage 41 as the intestine begins its first leftward curvature (Fig. 7). The tissue occluding the mouth begins to break down between NF stages 40 and 41, and at NF stage 42 the common foregut tube is completely divided with the trachea and lungs
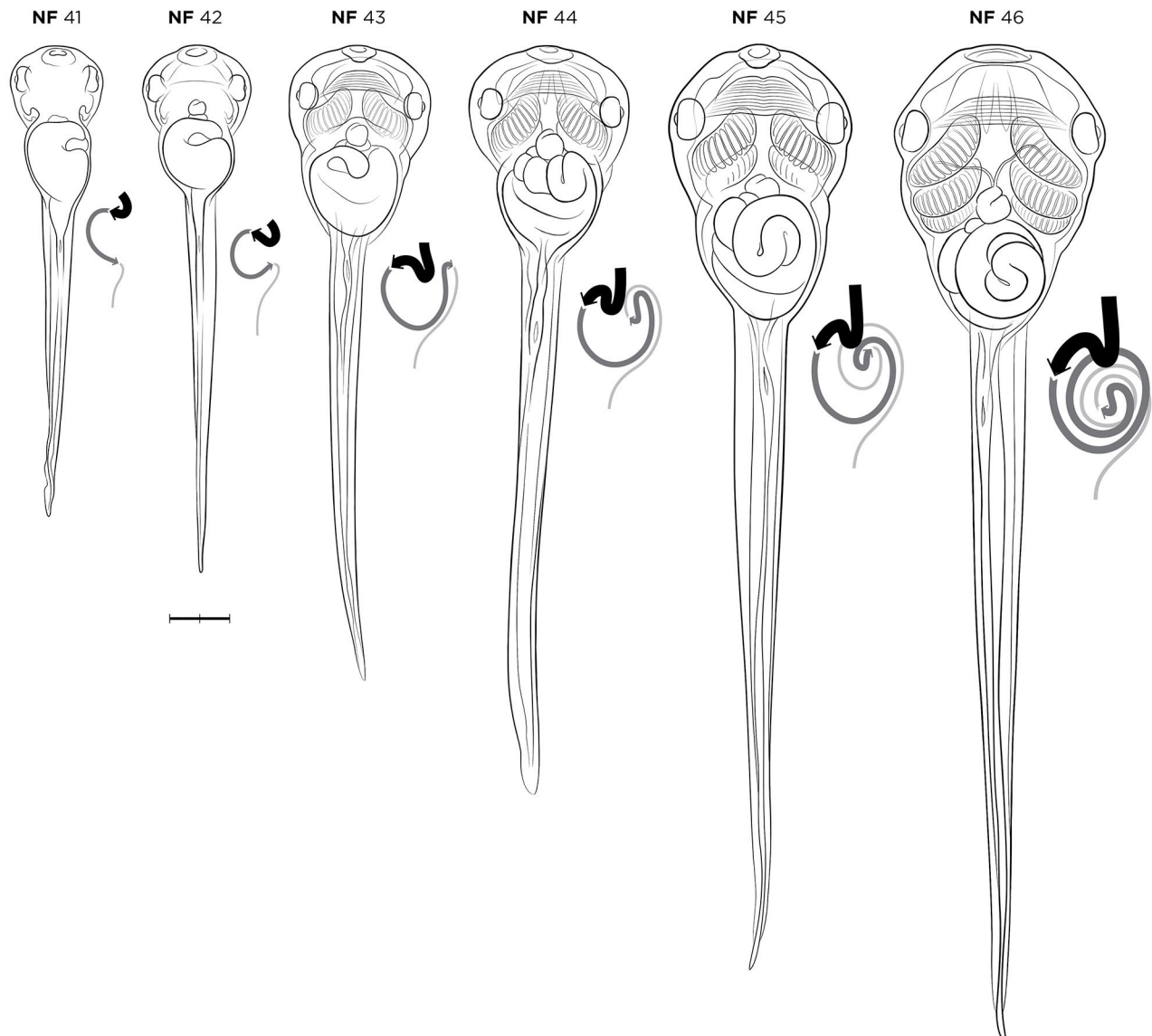

Fig. 7. *X. laevis* embryos during gut-coiling stages, NF stages 41-46, in ventral view, alongside new gut coiling diagrams. The coiling digestive tract is depicted as three lines of varying thickness. The esophagus/stomach (thickest black line) begins anteriorly on the left side of the body at NF stage 41. As gut lengthening and coiling progresses, the stomach shifts to the right side of the body by NF stage 46. The midgut (dark-gray line) and hindgut (thin light-gray line) form a rudimentary 'S' shape curve by NF stage 41-42, and at NF stage 43 the midgut and hindgut have lengthened to form a 'hairpin loop', visible from the left side. This loop turns ventrally by NF stage 44, becoming the U-shaped apex of the future intestinal coils. Throughout NF stages 44 to 46, the midgut and hindgut continue to lengthen and loop, with the apex rotating inward to form a compact intestine with tightly wound, counterclockwise coils. Gut-coiling diagrams designed by J.G. Stages as indicated. Scale bar: 1 mm.

separated from the esophagus (Nasr et al., 2019). Tadpoles start to feed at NF stage 45 (Fig. 6C) and food can be seen in the gut. As gut development and elongation proceeds through NF stages 43-47 (Figs 6B,C and 7), stereotypical gut coiling and asymmetry of the viscera/organs is best viewed ventrally.

New drawings of stages NF 41-46 in ventral view, alongside the new gut-coiling diagrams are shown in Fig. 7. The coiling digestive tract is depicted as three shaded lines of varying thickness, representing the foregut, midgut and hindgut. The esophagus/stomach (thick, black line) begins on the left side of the body at NF stage 41, lengthening extensively to situate the stomach on the right side of the body by NF stage 46. By NF stages 41-42, the midgut (dark-gray line) and hindgut (thin, light-gray line) form a rudimentary S-shaped curve. By NF stage 43, the midgut and hindgut have lengthened to form a 'hairpin loop' visible from the left side. This loop turns ventrally by NF stage 44, and will become the U-shaped apex (i.e. center) of the future intestinal coils. Between NF stages 44 and 46, the midgut and hindgut continue to lengthen, with the apex rotating inward to form an intestine with tightly wound, counter-clockwise coils.

Other landmarks at NF stages 44-46 involve skeletal growth, neural development and the visual system. Retinal ganglion cells reach the optic tectum and begin to form complex synapses in a stage-specific manner during NF stages 44-46 (Pratt, 2021). Visual avoidance behavior, whereby tadpoles swim away from dark spots/shadows, is first observed at NF stage 44 (Dong et al., 2009). At the end of the gut-coiling stages, the hindlimbs develop first, emerging as tiny crescent-shaped buds at NF stage 46 (although they can be difficult to see) and chondrification of the otic vesicle and parts of the skeleton begin to develop as the notochord starts to degenerate.

NF stages 47-61: premetamorphosis and prometamorphosis

Amphibian metamorphosis involves numerous, precisely timed developmental changes, including intestinal remodeling, limb growth, vascular reorganization, changes to the neuronal circuitry, tail resorption, simultaneous gill resorption and lung maturation, and the change from ciliated larval epidermis to adult skin (Brown and Cai, 2007; Choi et al., 2017; Tasca et al., 2021). The three phases of metamorphosis (premetamorphosis, prometamorphosis and climax metamorphosis) are represented by NF stages 48-59 (Figs 8A,B, 9 and 10A), NF stage 63 (tailed froglet; Fig. 10B) and NF stage 66 (froglet with a fully resorbed tail; Fig. 10C). Additional ventral views of these stages are available on Xenbase.

Landmarks for premetamorphosis (NF stages 47-54) focus on limb growth and increasing numbers of pigmented melanophores (Table S1). At NF stage 47, the 'atria', where forelimb will develop, is formed; however, forelimb buds are not visible until NF stage 50 (Fig. 8). At NF stage 52 (Fig. 9A), the hindlimb has an indented wrist, and by NF stage 54 (Fig. 9B) the foot forms as a splayed paddle with five thickened digits and thinner inter-digital webbing. At the molecular level, *fgf8*, *fgf2* and *sall4* are widely used markers for hindlimb bud, and *fgf2* for the forelimb bud. Melanophores form an opaque layer surrounding the abdominal cavity and the intestinal coils at NF stage 47, and these become iridescent gold by NF stage 48. Additional landmarks for these stages include the developing brain, where the axon tracts forming between the retinal ganglionic cells and the optic tectum develop in a stage-specific progression (Liu et al., 2016). Furthermore, tadpoles at late premetamorphosis stages are regeneration competent, in that full regeneration of a lost tail or limbs is possible (Aztekin et al., 2021).
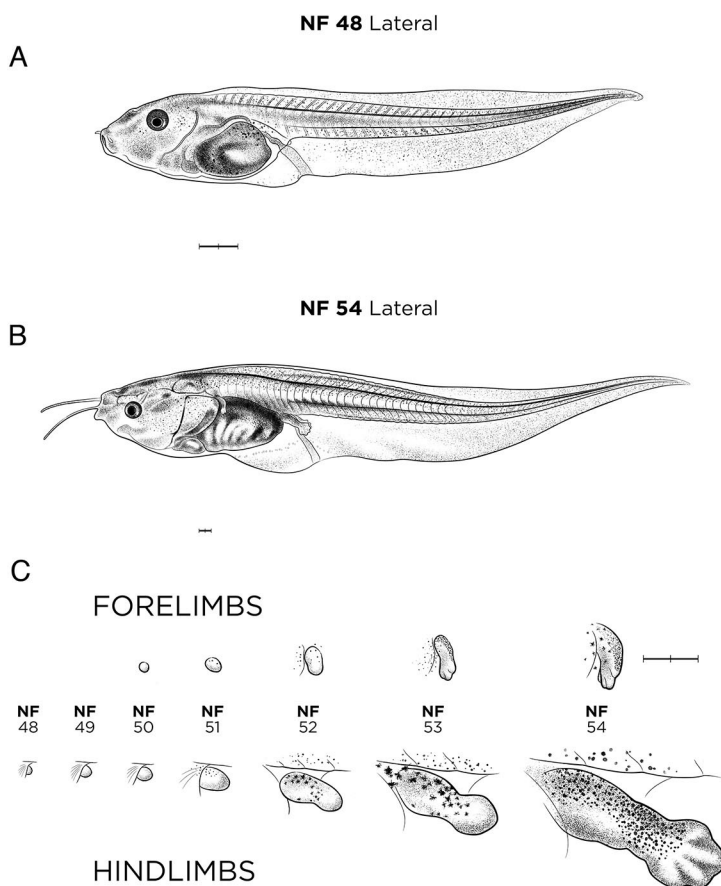
Fig. 8. Limb development in *X. laevis* tadpoles. (A) NF stage 48 tadpole. (B) NF stage 54. (C) Limb bud development from NF stage 48 to 54, reproduced in the style of the drawing in the Nieuwkoop and Faber Normal Table (Nieuwkoop and Faber, 1956, 1994), but in left-to-right progression, with forelimbs (above) and hindlimbs (below), at the stages indicated. See Table S1 for staging landmarks. Views as indicated. Scale bars: 1 mm.
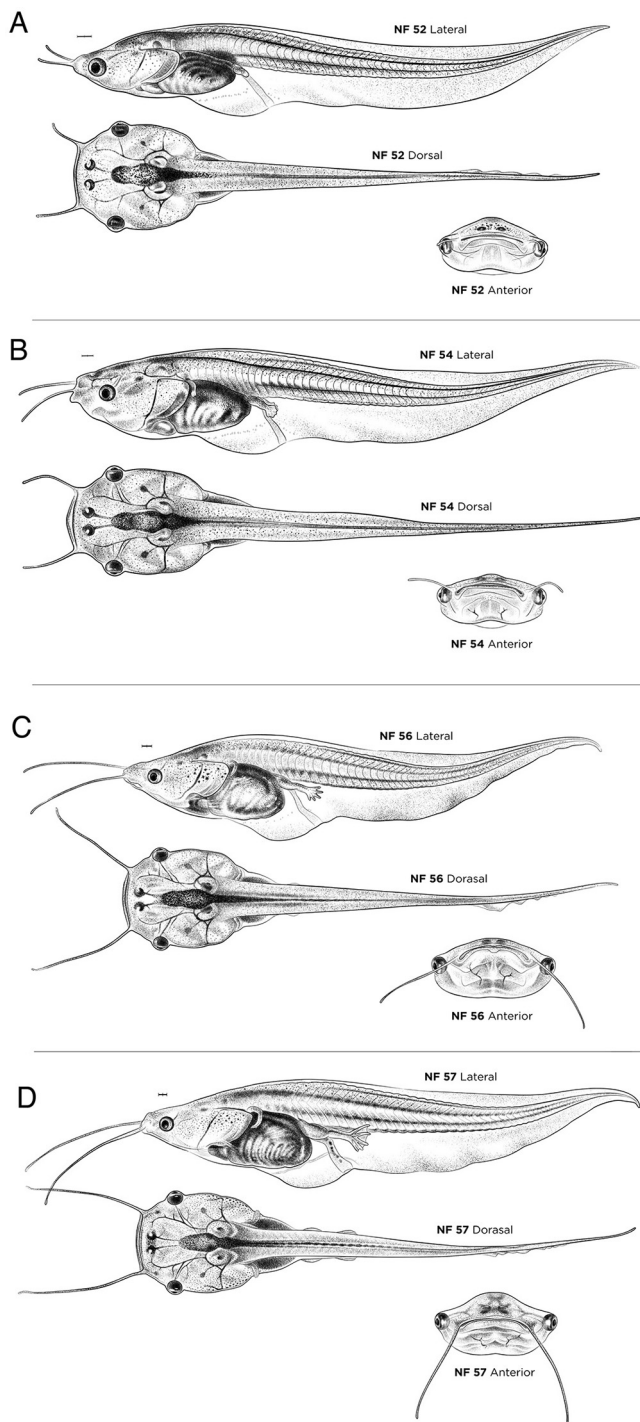
NF 48 Lateral

A

NF 54 Lateral

B

C

FORELIMBS

| NF 48 | NF 49 | NF 50 | NF 51 | NF 52 | NF 53 | NF 54 |

HINDLIMBS

Fig. 9. Premetamorphosis- and prometamorphosis-stage *X. laevis* tadpoles. (A) NF stage 52 (premetamorphosis). (B) NF stage 54 (premetamorphosis). (C) NF stage 56 (prometamorphosis). (D) NF stage 57, (prometamorphosis). Each stage is shown in lateral, dorsal and anterior views. Ventral views are available on Xenbase. See Table S1 for more staging landmarks. Membrane removed in all embryos. Views as indicated. Scale bars: 1 mm.

During prometamorphosis (NF stages 55-61), the respiratory system changes from gills to lungs and the limb musculature and skeleton mature. The relative proportions of limb segments and the position of the growing limbs are used as key staging landmarks. At NF stage 55 (not shown), the forelimb hand rotates 90° and the

digits/fingers are as long as they are wide. At NF stage 56 (Fig. 9C), the hindlimbs start to be visible from above because they can rotate away from body. At NF stage 57 (Fig. 9D), the forelimb is still covered by the operculum membrane. Tadpoles at NF stage 55-56 are considered 'regeneration restricted' in that complete regeneration of a limb is no longer possible, and at NF stage 58 onwards tadpoles are completely 'regeneration incompetent' (Aztekin et al., 2021).

Levels of the thyroid hormones (TH) thyroxine (T_4) and 3,5,3′-l-triiodothyronine (T_3) are the key driver of metamorphosis (Table S1). First detectable at NF stage 47, TH levels dramatically increase from NF stage 54 (Fig. 8B) to NF stages 55-61, peaking at NF stage 62-63 (Fig. 10B), and returning to prometamorphic levels by NF stage 66 (Fig. 10C) (Buchholz and Shi, 2018).

NF stages 58-66: climax of metamorphosis

Climax of metamorphosis, when tail and the gills are resorbed, culminates in an air-breathing, yet still fully aquatic, *Xenopus* froglet. At NF stage 58, ~44 days after fertilization at 23°C, the forelimbs erupt, usually elbows first (although left and right forelimbs may not emerge simultaneously), and the claws form on the tips of hindlimb digit tips (they are white at first). At NF stage 59 (Fig. 10A), the hindlimb claws (from which the species gets its common name) turn hard and black, the shortest toes first, and the sensory barbels begin to shrivel up. A common molecular marker for the cartilage elements of developing digits is *sox9*, whereas *tbx4* and *sall4* mark the interdigital mesenchyme (Neff et al., 2005). By NF stage 61, both hindlimb and forelimb are fully formed, the adult skin has developed across the body, and tadpoles cease feeding owing to oral and intestinal remodeling (Choi et al., 2017). Significant changes in the shape of the head, relative position of the mouth and eyes, and the natural positions of the limbs can be observed by comparing NF stage 63 (Fig. 10B) and NF stage 66 (Fig. 10C), many of which are useful staging landmarks.

DISCUSSION

We have created a new open-source set of illustrations showing the Normal Table of *Xenopus* development from fertilization through embryonic development, to fully metamorphosized froglet, to be used in conjunction with text of the classic Nieuwkoop and Faber Normal Table (Nieuwkoop and Faber, 1994) and the histology atlas of Hausen and Riebesell (1991). This new online digital resource, with images in the classic Nieuwkoop and Faber style, will overcome the current limitations in reusing the original illustrations, whereby it is impossible to obtain reuse copyright permission. The new Zahn collection also includes additional views that were not presented in the original Normal Table, but are valuable for current research. We also include line diagrams of some key stages, such as cleavage and blastula, which are frequently modified and reused to illustrate experimental design in scientific papers.

Continuous morphological change is a natural feature of development, and, in practice, applying staging criterion is challenging, even for experts. When designing experiments, researchers can either wait until an easy-to-determine stage is reached, or halt experiments at a set time point and then 'stage' the embryos. Our Landmarks Table (Table S1) provides a succinct guide that can be used by experts and the inexperienced alike, to stage embryos quickly and reliably. The Landmarks Table not only includes external morphology, but also internal anatomical landmarks based on descriptions in the Nieuwkoop and Faber Normal Table (Nieuwkoop and Faber, 1994) and the histological images in Hausen and Riebesell (1991), with input from the *Xenopus*
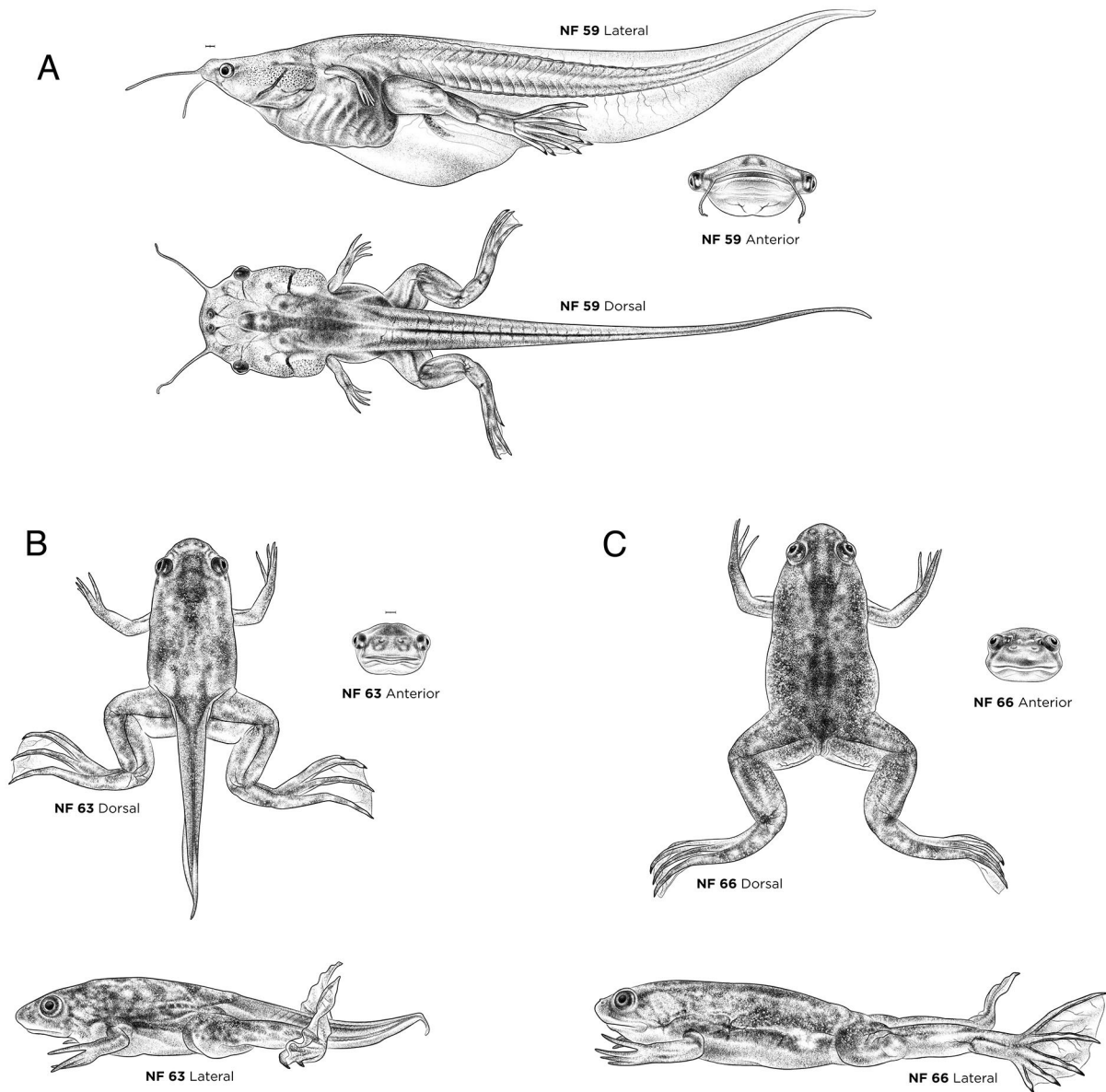
Fig. 10. Prometamorphosis- and climax metamorphosis-stage *X. laevis* tadpoles. (A) NF stage 59. (B) NF stage 63. (C) NF stage 66. Each stage is shown in lateral, dorsal and anterior views. Ventral views are available on Xenbase. See Table S1 for more staging landmarks. Membrane removed in all embryos. Views as indicated. Scale bars: 1 mm.

community. Finally, the stage- and tissue-specific molecular markers were curated from decades of *Xenopus* research data in Xenbase.

The experimental advantages of *Xenopus* include a well-defined fate map, targeted microinjection, experimental embryology, rapid CRISPR-gene editing, transgenics and older tadpoles that are largely transparent making it easy to observe organogenesis in real time. As a result, *X. laevis* and *X. tropicalis* are used to model an increasing variety of human diseases affecting various organ systems as well as to elucidate basic principles of cell biology, genomics and morphogenesis, while informing advances in stem cell and organoid technology, injury, repair and regeneration, and toxicology (Sater and Moody, 2017; Nenni et al., 2019; Hoppler and Conlon, 2020; Gao and Shen, 2021). All disease modeling studies rely on accurate, reproducible staging and an understanding of a normal wild-type *Xenopus* phenotype. The Zahn drawing series provides a realistic, highly detailed study of anatomically 'normal'

embryos and tadpoles, by which 'abnormal' phenotypes can be assessed. The new anterior views of tadpoles, for example, may be a particularly useful reference to assess craniofacial defects, for which it is important to assess the relative positioning of the mouth, nose and eyes (Wyatt et al., 2021b).

The new ventral views of *Xenopus* tadpoles from NF stages 41-46 and diagrams of gut coiling will enable researchers to model more accurately congenital defects of the digestive system and visceral organs, such as situs inversus, heterotaxia, straight or shortened gut, reversed intestinal coiling or malrotation (Bergmann et al., 2008; Gur et al., 2017; Dush and Nascone-Yoder, 2019; Wyatt et al., 2021a). The gut-coiling diagrams will also facilitate the use of *Xenopus* for toxicology research, as digestive tract phenotypes are a common outcome of the 'Frog Embryo Teratogenesis Assay *Xenopus*' (FETAX), an industry standard used to assess the developmental toxicity of pharmaceuticals and food supplements

(Islas-Flores et al., 2018; Fort and Mathis, 2018; Battistoni et al., 2020), agricultural chemicals (Babalola et al., 2021) and other pollutants (Mouche et al., 2017; Xu et al., 2019). FETAX phenotypes are generally assessed by whole-mount microscopy of late tadpole stages; however, most studies use simple 'gut malformations' or 'abnormal gut coiling' categories for phenotypes. Given that gut phenotypes can be complex, the new ventral views and gut-coiling diagrams will help researchers understand digestive system development in the frog and will enable more accurate descriptions of gut phenotypes. Similarly, we predict this work will aid the staging of embryos for phenotype scoring for EAMA and AMA (Extended/Amphibian Metamorphosis Assay). EAMA and AMA assess the effects of potential endocrine and thyroid pathway disrupting substances on amphibian metamorphosis, by scoring limb phenotypes, abnormal behavior, time to metamorphosis, and mortality during prometamorphosis and climax metamorphosis stages (Dang, 2019; Ortego et al., 2021).

In modern times, normal tables of development have provided the basis for more systematic annotation of biological data using ontologies, controlled vocabularies that make data machine readable and thus enable computational analysis (Hunter et al., 2003; Van Slyke et al., 2014; Bard, 2012; Slater et al., 2020). In Xenbase, developmental stages, cell types, tissues and organs are represented in the *Xenopus* Anatomical Ontology (the XAO), with term definitions being directly adapted from the Normal Table (e.g. NF stage 42 is XAO ID:l1000054) (Segerdell et al., 2013). The XAO is used to describe gene expression patterns and is the foundation for the *Xenopus* Phenotype Ontology (the XPO), which is used to describe experimental phenotypes and link these phenotypes to human disease (Fisher et al., 2021). On Xenbase, the new Zahn drawings also illustrate the XAO pages for the NF stages, and researchers can explore stage-specific gene expression data. The online version of the Landmarks Table on Xenbase (https://www.xenbase.org/entry/landmarks-table.do) has live links that direct researchers to (1) gene pages, with links to extensive gene-specific expression data, genomic resources and orthologs, and to (2) XAO pages, with tissue-specific gene expression data (Figs S2 and S3). Researchers can use Xenbase search tools to interrogate and efficiently connect anatomical development to curated data (gene expression, phenotypes and associated diseases) and primary literature sources (James-Zorn et al., 2018). Importantly, this online version of the Normal Table will be a dynamic, evolving resource that can be updated with the latest molecular data attributed to different stages and tissues.

In summary, we hope that these new open-source online resources will encourage and enhance exploration of the classic Nieuwkoop and Faber Normal Table of *Xenopus* development. We anticipate that the new Zahn images and their integration on Xenbase will facilitate the ongoing renaissance of *Xenopus* research in the genomics of human disease modeling. Finally, we hope that releasing the Zahn images as an open-access resource will support educators teaching the next generation of embryology students and *Xenopus* researchers.

MATERIALS AND METHODS
Producing the illustrations
The method of producing this new set of illustrations began with observations of live specimens under a stereomicroscope, sketching and photographing specimens to produce reference images.

This process was essentially the same as that described previously (Zahn et al., 2017). Animals used in this project were wild-type J-strain *X. laevis* (NXR_0.0024), accessed at the National *Xenopus* Resource (NXR; RRID: SCR_013731) at the Marine Biology Laboratory (MBL) at Woods Hole, MA, USA. Animals were handled following the ARRIVE and NIH

Guidelines for Use and Care of Laboratory Animals that were approved by the Institutional Animal Care and Use Committee of the MBL. Representative embryos from several different clutches were used. The developmental stages were prior to overt sexual identification. Vitelline membranes were removed from embryos at NF stages 13-15, because if not removed, the membrane flattens the neural plate, making it more difficult to tell NF stages 13-15 apart (Sive et al., 2007a). Likewise, the membranes were removed from stage NF 22-35 tailbud embryos before photographing to remove the curve in the body axis. Swimming tadpoles were anesthetized using approved methods. Specimens were photographed using a Zeiss steREO Discovery.V12 microscope with an AxioCam MRc camera. Larger tadpoles and froglets were imaged with an Apple iPhone XR camera.

Draft drawings were assessed by the authors (A.M.Z., S.A.M., P.D.V., D.R.B., D.S.A., N.M.N.-Y., J.G.), all experienced domain experts, to ensure that they illustrated stereotypical anatomical features, and additional reference images were all provided to the illustrator from our labs (A.M.Z., S.A.M., D.R.B., N.M.N.-Y.). Additional high-resolution reference images of staged embryos were kindly provided by the *Xenopus* community [e.g. the Willsey Laboratory (University of California, San Francisco, CA, USA) provided dorsal views of late-stage tadpoles showing brain morphology; and we used Kirschner Laboratory (Harvard Medical School, MA, USA) and other images posted in the *Xenopus* community Slack forum]. In addition to the fully shaded illustrations, simple line drawings and outlines for many of the stages were also drawn (Fig. S1). New diagrams of the gut coiling process (by J.G. and N.Z.) accompany ventral views of NF stages 41-46, illustrating the shape and directionality of this dynamic process. Gut coiling diagrams were based on anatomical studies of the *Xenopus* alimentary system, for which tadpoles were anesthetized and/or euthanized in accordance with North Carolina State University Institutional Animal Care and Use Committee regulations. Final versions of all illustrations were produced in a digital format using applications from Adobe's Creative Suite and a Wacom Cintiq Pro 32 digital drawing display. All drawings are provided as 300 dpi, high-resolution pixel-based art, and include a scale bar and, where applicable, a compass rose, indicating size and orientation, respectively.

Accessing Zahn drawings on Xenbase
The Zahn drawings presented here and those from the XenHead project (Zahn et al., 2017) are available as individual digital files (jpg format) and as a compiled printable sheet (pdf format) on Xenbase in the Anatomy & Development module (http://www.xenbase.org/entry/zahn.do). Additionally, the Zahn drawings are used to illustrate the XAO pages (http://www.xenbase.org/anatomy/xao.do?method=display) for relevant NF stages (Fig. S2).

DEVELOPMENT

Data availability
All the Zahn drawings (those presented here and the earlier XenHead set) are available on Xenbase (http://www.xenbase.org/entry/zahn.do) through an attributable, non-commercial creative commons license (CC BY-NC 4.0). To reproduce any of these images please use the following attribution: Illustration © 2021 Natalya Zahn, CC BY-NC 4.0, and cite Xenbase (http://www.xenbase.org, RRID:SCR_003280) and this article. This license permits reuse and manipulation of up to six illustrations, for any noncommercial use, with the attribution above. To use more illustrations, or for any commercial use, contact the illustrator, Natalya Zahn (email:natalya@natalya.com) for permission (fees may apply). Further information is available on the Xenbase page, and full details of the license can be read here: https://creativecommons.org/licenses/by-nc/4.0/?ref=chooser-v1. Note that the full series of original Nieuwkoop and Faber drawings and the entire set of histology plates from Hausen and Riebesell (1991) are also available on Xenbase in the Anatomy and Development module.

Poster
A poster of the Zahn drawings showing key stages of *Xenopus* development is available as supplementary material in the online version of this article at https://journals.biologists.com/dev/article-lookup/DOI/10.1242/dev.200356.

Peer review history
The peer review history is available online at https://journals.biologists.com/dev/article-lookup/doi/10.1242/dev.200356.

References
Almasoudi, S. H. and Schlosser, G. (2021). Otic neurogenesis in *Xenopus laevis*: proliferation, differentiation, and the role of Eya1. *Front. Neuroanat.* **15**, 722374. doi:10.3389/fnana.2021.722374

Aztekin, C., Hiscock, T. W., Gurdon, J., Jullien, J., Marioni, J. and Simons, B. D. (2021). Secreted inhibitors drive the loss of regeneration competence in *Xenopus* limbs. *Development* **148**, dev199158. doi:10.1242/dev.199158

Babalola, O. O., Truter, J. C. and Van Wyk, J. H. (2021). Lethal and teratogenic impacts of imazapyr, diquat dibromide, and glufosinate ammonium herbicide formulations using frog embryo teratogenesis assay-*Xenopus* (FETAX). *Arch. Environ. Contam. Toxicol.* **80**, 708-716. doi:10.1007/s00244-020-00756-5

Bard, J. (2012). A new ontology (structured hierarchy) of human developmental anatomy for the first 7 weeks (Carnegie stages 1-20). *J. Anat.* **221**, 406-416. doi:10.1111/j.1469-7580.2012.01566.x

Battistoni, M., Bacchetta, R., Di Renzo, F., Metruccio, F. and Menegola, E. (2020). Effect of nano-encapsulation of beta-carotene on *Xenopus laevis* embryos development (FETAX). *Toxicol. Rep.* **7**, 510-519. doi:10.1016/j.toxrep.2020.04.004

Beckers, A., Fuhl, F., Ott, T., Boldt, K., Brislinger, M. M., Walentek, P., Schuster-Gossler, K., Hegermann, J., Alten, L., Kremmer, E. et al. (2021). The highly conserved FOXJ1 target CFAP161 is dispensable for motile ciliary function in mouse and *Xenopus*. *Sci. Rep.* **11**, 13333. doi:10.1038/s41598-021-92495-3

Bergmann, C., Fliegauf, M., Bruchle, N. O., Frank, V., Olbrich, H., Kirschner, J., Schermer, B., Schmedding, I., Kispert, A., Kranzlin, B. et al. (2008). Loss of nephrocystin-3 function can cause embryonic lethality, Meckel-Gruber-like syndrome, situs inversus, and renal-hepatic-pancreatic dysplasia. *Am. J. Hum. Genet.* **82**, 959-970. doi:10.1016/j.ajhg.2008.02.017

Betley, J. N., Frith, M. C., Graber, J. H., Choo, S. and Deshler, J. O. (2002). A ubiquitous and conserved signal for RNA localization in chordates. *Curr. Biol.* **12**, 1756-1761. doi:10.1016/S0960-9822(02)01220-4

Breckenridge, R. A., Mohun, T. J. and Amaya, E. (2001). A role for BMP signalling in heart looping morphogenesis in *Xenopus*. *Dev. Biol.* **232**, 191-203. doi:10.1006/dbio.2001.0164

Brivanlou, A. H. and Harland, R. M. (1989). Expression of an engrailed-related protein is induced in the anterior neural ectoderm of early *Xenopus* embryos. *Development* **106**, 611-617. doi:10.1242/dev.106.3.611

Brown, D. D. and Cai, L. (2007). Amphibian metamorphosis. *Dev. Biol.* **306**, 20-33. doi:10.1016/j.ydbio.2007.03.021

Buchholz, D. R. and Shi, Y. B. (2018). Methods for investigating the larval period and metamorphosis in *Xenopus*. *Cold Spring Harb. Protoc.* **2018**, pdb.top097667. doi:10.1101/pdb.top097667

Choi, J., Ishizuya-Oka, A. and Buchholz, D. R. (2017). Growth, development, and intestinal remodeling occurs in the absence of thyroid hormone receptor alpha in tadpoles of *Xenopus tropicalis*. *Endocrinology* **158**, 1623-1633. doi:10.1210/en.2016-1955

Chung, M. I., Kwon, T., Tu, F., Brooks, E. R., Gupta, R., Meyer, M., Baker, J. C., Marcotte, E. M. and Wallingford, J. B. (2014). Coordinated genomic control of ciliogenesis and cell movement by RFX2. *Elife* **3**, e01439. doi:10.7554/eLife.01439

Cleaver, O., Tonissen, K. F., Saha, M. S. and Krieg, P. A. (1997). Neovascularization of the *Xenopus* embryo. *Dev. Dyn.* **210**, 66-77. doi:10.1002/(SICI)1097-0177(199709)210:1<66::AID-AJA7>3.0.CO;2-#

Dang, Z. (2019). Endpoint sensitivity in amphibian metamorphosis assay. *Ecotoxicol. Environ. Saf.* **167**, 513-519. doi:10.1016/j.ecoenv.2018.10.028

De Bakker, B. S., Van Den Hoff, M. J. B., Vize, P. D. and Oostra, R. J. (2019). The pronephros; a fresh perspective. *Integr. Comp. Biol.* **59**, 29-47. doi:10.1093/icb/icz001

Dong, W., Lee, R. H., Xu, H., Yang, S., Pratt, K. G., Cao, V., Song, Y. K., Nurmikko, A. and Aizenman, C. D. (2009). Visual avoidance in *Xenopus* tadpoles is correlated with the maturation of visual responses in the optic tectum. *J. Neurophysiol.* **101**, 803-815. doi:10.1152/jn.90848.2008

Drysdale, T. A., Tonissen, K. F., Patterson, K. D., Crawford, M. J. and Krieg, P. A. (1994). Cardiac troponin I is a heart-specific marker in the *Xenopus* embryo: expression during abnormal heart morphogenesis. *Dev. Biol.* **165**, 432-441. doi:10.1006/dbio.1994.1265

Durston, A. J., Timmermans, J. P., Hage, W. J., Hendriks, H. F., De Vries, N. J., Heideveld, M. and Nieuwkoop, P. D. (1989). Retinoic acid causes an anteroposterior transformation in the developing central nervous system. *Nature* **340**, 140-144. doi:10.1038/340140a0

Dush, M. K. and Nascone-Yoder, N. M. (2019). Vangl2 coordinates cell rearrangements during gut elongation. *Dev. Dyn.* **248**, 569-582. doi:10.1002/dvdy.61

Fisher, M. E., Segerdell, E., Matentzoglu, N., Nenni, M. J., Fortriede, J. D., Chu, S., Pells, T. J., Osumi-Sutherland, D., Chaturvedi, P., James-Zorn, C. et al. (2022). The Xenopus phenotype ontology: bridging model organism phenotype data to human health and development. *BMC Bioinformatics* **23**, 99. doi:10.1186/s12859-022-04636-8

Fletcher, R. B. and Harland, R. M. (2008). The role of FGF signaling in the establishment and maintenance of mesodermal gene expression in Xenopus. *Dev. Dyn.* **237**, 1243-1254. doi:10.1002/dvdy.21517

Fort, D. J. and Mathis, M. (2018). Frog embryo teratogenesis Assay-*Xenopus* (FETAX): use in alternative preclinical safety assessment. *Cold Spring Harb. Protoc.* **2018**. doi:10.1101/pdb.prot098319

Gao, J. and Shen, W. (2021). *Xenopus* in revealing developmental toxicity and modeling human diseases. *Environ. Pollut.* **268**, 115809. doi:10.1016/j.envpol.2020.115809

Gawantka, V., Pollet, N., Delius, H., Vingron, M., Pfister, R., Nitsch, R., Blumenstock, C. and Niehrs, C. (1998). Gene expression screening in *Xenopus* identifies molecular pathways, predicts gene function and provides a global view of embryonic patterning. *Mech. Dev.* **77**, 95-141. doi:10.1016/S0925-4773(98)00115-4

Gur, M., Cohen, E. B.-T., Genin, O., Fainsod, A., Perles, Z. and Cinnamon, Y. (2017). Roles of the cilium-associated gene CCDC11 in left-right patterning and in laterality disorders in humans. *Int. J. Dev. Biol.* **61**, 267-276. doi:10.1387/ijdb.160442yc

Hausen, P. and Riebesell, M. (1991). *The early development of Xenopus Laevis: an atlas of the histology*. Verlag der Zeitschrift für Naturforschung, Tügingen.

Heller, N. and Brändli, A. W. (1997). *Xenopus* Pax-2 displays multiple splice forms during embryogenesis and pronephric kidney development. *Mech. Dev.* **69**, 83-104. doi:10.1016/S0925-4773(97)00158-5

Hoppler, S. and Conlon, F. L. (2020). *Xenopus*: experimental access to cardiovascular development, regeneration discovery, and cardiovascular heart-defect modeling. *Cold Spring Harb. Perspect Biol* **12**, a037200. doi:10.1101/cshperspect.a037200

Hopwood, N. (2007). A history of normal plates, tables and stages in vertebrate embryology. *Int. J. Dev. Biol.* **51**, 1-26. doi:10.1387/ijdb.062189nh

Hopwood, N. D., Pluck, A., Gurdon, J. B. and Dilworth, S. M. (1992). Expression of XMyoD protein in early Xenopus laevis embryos. *Development* **114**, 31-38. doi:10.1242/dev.114.1.31

Hunter, A., Kaufman, M. H., McKay, A., Baldock, R., Simmen, M. W. and Bard, J. B. (2003). An ontology of human developmental anatomy. *J. Anat.* **203**, 347-355. doi:10.1046/j.1469-7580.2003.00224.x

Illes, J. C., Winterbottom, E. and Isaacs, H. V. (2009). Cloning and expression analysis of the anterior parahox genes, Gsh1 and Gsh2 from *Xenopus tropicalis*. *Dev. Dyn.* **238**, 194-203. doi:10.1002/dvdy.21816

Islas-Flores, H., Pérez-Alvarez, I. and Gómez-Oliván, L. M. (2018). Evaluation of teratogenicity of pharmaceuticals using FETAX. *Methods Mol. Biol.* **1797**, 299-307. doi:10.1007/978-1-4939-7883-0_15

James-Zorn, C., Ponferrada, V., Fisher, M. E., Burns, K., Fortriede, J., Segerdell, E., Karimi, K., Lotay, V., Wang, D. Z., Chu, S. et al. (2018). Navigating Xenbase: an integrated *Xenopus* genomics and gene expression database. *Methods Mol. Biol.* **1757**, 251-305. doi:10.1007/978-1-4939-7737-6_10

Kazanskaya, O., Ohkawara, B., Heroult, M., Wu, W., Maltry, N., Augustin, H. G. and Niehrs, C. (2008). The Wnt signaling regulator R-spondin 3 promotes angioblast and vascular development. *Development* **135**, 3655-3664. doi:10.1242/dev.027284

Keller, R. and Sutherland, A. (2020). Convergent extension in the amphibian, *Xenopus laevis*. *Curr. Top. Dev. Biol.* **136**, 271-317. doi:10.1016/bs.ctdb.2019.11.013

Kelley, C., Yee, K., Harland, R. and Zon, L. I. (1994). Ventral expression of GATA-1 and GATA-2 in the *Xenopus* embryo defines induction of hematopoietic mesoderm. *Dev. Biol.* **165**, 193-205. doi:10.1006/dbio.1994.1246

Kennedy, A. E. and Dickinson, A. J. (2012). Median facial clefts in *Xenopus laevis*: roles of retinoic acid signaling and homeobox genes. *Dev. Biol.* **365**, 229-240. doi:10.1016/j.ydbio.2012.02.033

Khokha, M. K., Chung, C., Bustamante, E. L., Gaw, L. W., Trott, K. A., Yeh, J., Lim, N., Lin, J. C., Taverner, N., Amaya, E. et al. (2002). Techniques and probes for the study of *Xenopus tropicalis* development. *Dev. Dyn.* **225**, 499-510. doi:10.1002/dvdy.10184

Kuriyama, S. and Mayor, R. (2008). Molecular analysis of neural crest migration. *Philos. Trans. R. Soc. Lond. B Biol. Sci.* **363**, 1349-1362. doi:10.1098/rstb.2007.2252

Kuriyama, S. and Mayor, R. (2009). A role for Syndecan-4 in neural induction involving ERK- and PKC-dependent pathways. *Development* **136**, 575-584. doi:10.1242/dev.027334

Lea, R., Papalopulu, N., Amaya, E. and Dorey, K. (2009). Temporal and spatial expression of FGF ligands and receptors during *Xenopus* development. *Dev. Dyn.* **238**, 1467-1479. doi:10.1002/dvdy.21913

Li, L., Wen, L., Gong, Y., Mei, G., Liu, J., Chen, Y. and Peng, T. (2012). *Xenopus* as a model system for the study of GOLPH2/GP73 function: *Xenopus* GOLPH2 is required for pronephros development. *PLoS One* **7**, e38939. doi:10.1371/journal.pone.0038939

Liu, Z., Hamodi, A. S. and Pratt, K. G. (2016). Early development and function of the *Xenopus* tadpole retinotectal circuit. *Curr. Opin. Neurobiol.* **41**, 17-23. doi:10.1016/j.conb.2016.07.002

Moosmann, J., Ershov, A., Altapova, V., Baumbach, T., Prasad, M. S., Labonne, C., Xiao, X., Kashef, J. and Hofmann, R. (2013). X-ray phase-contrast in vivo microtomography probes new aspects of *Xenopus* gastrulation. *Nature* **497**, 374-377. doi:10.1038/nature12116

Mouche, I., Malesic, L. and Gillardeaux, O. (2017). FETAX Assay for evaluation of developmental toxicity. *Methods Mol. Biol.* **1641**, 311-324. doi:10.1007/978-1-4939-7172-5_17

Nakayama, T., Fisher, M., Nakajima, K., Odeleye, A. O., Zimmerman, K. B., Fish, M. B., Yaoita, Y., Chojnowski, J. L., Lauderdale, J. D., Netland, P. A. et al. (2015). *Xenopus pax6* mutants affect eye development and other organ systems, and have phenotypic similarities to human aniridia patients. *Dev. Biol.* **408**, 328-344. doi:10.1016/j.ydbio.2015.02.012

Nasr, T., Mancini, P., Rankin, S. A., Edwards, N. A., Agricola, Z. N., Kenny, A. P., Kinney, J. L., Daniels, K., Vardanyan, J., Han, L. et al. (2019). Endosome-mediated epithelial remodeling downstream of hedgehog-Gli is required for tracheoesophageal separation. *Dev. Cell* **51**, 665-674.e6. doi:10.1016/j.devcel.2019.11.003

Neff, A. W., King, M. W., Harty, M. W., Nguyen, T., Calley, J., Smith, R. C. and Mescher, A. L. (2005). Expression of *Xenopus* XlSALL4 during limb development and regeneration. *Dev. Dyn.* **233**, 356-367. doi:10.1002/dvdy.20363

Nenni, M. J., Fisher, M. E., James-Zorn, C., Pells, T. J., Ponferrada, V., Chu, S., Fortriede, J. D., Burns, K. A., Wang, Y., Lotay, V. S. et al. (2019). Xenbase: facilitating the Use of *Xenopus* to model human disease. *Front. Physiol.* **10**, 154. doi:10.3389/fphys.2019.00154

Newport, J. and Kirschner, M. (1982). A major developmental transition in early *Xenopus* embryos: I. characterization and timing of cellular changes at the midblastula stage. *Cell* **30**, 675-686. doi:10.1016/0092-8674(82)90272-0

Nieuwkoop, P. D. (1973). The organization center of the amphibian embryo: its origin, spatial organization, and morphogenetic action. *Adv. Morphog.* **10**, 1-39. doi:10.1016/B978-0-12-028610-2.50005-8

Nieuwkoop, P. D. (1985). Inductive interactions in early amphibian development and their general nature. *J. Embryol. Exp. Morphol.* **89**, 333-347. doi:10.1242/dev.89.Supplement.333

Nieuwkoop, P. D. and Faber, J. (1956). *Normal Table of Xenopus laevis (Daudin); a Systematical and Chronological Survey of the Development from the Fertilized Egg Till the End of Metamorphosis*. Amsterdam: Hubrecht-Laboratorium (Embryologisch Instituut), North-Holland Pub. Co.

Nieuwkoop, P. D. and Faber, J. (1994). *Normal Table of Xenopus laevis (Daudin): a Systematical and Chronological Survey of the Development from the Fertilized Egg Till the end of Metamorphosis*. New York: Garland Pub.

Ortego, L. S., Olmstead, A. W., Weltje, L., Wheeler, J. R., Bone, A. J., Coady, K. K., Banman, C. S., Burden, N. and Lagadic, L. (2021). The extended amphibian metamorphosis assay: a thyroid-specific and less animal-intensive alternative to the larval amphibian growth and development assay. *Environ. Toxicol. Chem.* **40**, 2135-2144. doi:10.1002/etc.5078

Pan, F. C., Chen, Y., Bayha, E. and Pieler, T. (2007). Retinoic acid-mediated patterning of the pre-pancreatic endoderm in *Xenopus* operates via direct and indirect mechanisms. *Mech. Dev.* **124**, 518-531. doi:10.1016/j.mod.2007.06.003

Parain, K., Mazurier, N., Bronchain, O., Borday, C., Cabochette, P., Chesneau, A., Colozza, G., El Yakoubi, W., Hamdache, J., Locker, M. et al. (2012). A large scale screen for neural stem cell markers in Xenopus retina. *Dev. Neurobiol.* **72**, 491-506. doi:10.1002/dneu.20973

Park, B. Y., Hong, C.-S., Sohail, F. A. and Saint-Jeannet, J.-P. (2009). Developmental expression and regulation of the chemokine CXCL14 in Xenopus. *Int. J. Dev. Biol.* **53**, 535-540. doi:10.1387/ijdb.092855bp

Pratt, K. G. (2021). Electrophysiological approaches to studying normal and abnormal retinotectal circuit development in the Xenopus tadpole. *Cold Spring Harb Protoc*. pdb.prot106898. doi:10.1101/pdb.prot106898

Raciti, D., Reggiani, L., Geffers, L., Jiang, Q., Bacchion, F., Subrizi, A. E., Clements, D., Tindal, C., Davidson, D. R., Kaissling, B. et al. (2008). Organization of the pronephric kidney revealed by large-scale gene expression mapping. *Genome Biol.* **9**, R84. doi:10.1186/gb-2008-9-5-r84

Rankin, S. A., Thi Tran, H., Wlizla, M., Mancini, P., Shifley, E. T., Bloor, S. D., Han, L., Vleminckx, K., Wert, S. E. and Zorn, A. M. (2015). A molecular atlas of Xenopus respiratory system development. *Dev. Dyn.* **244**, 69-85. doi:10.1002/dvdy.24180

Roelink, H., Augsburger, A., Heemskerk, J., Korzh, V., Norlin, S., Altaba, R. I., Tanabe, A., Placzek, Y., Edlund, M., Jessell, T., et al. (1994). Floor plate and motor neuron induction by vhh-1, a vertebrate homolog of hedgehog expressed by the notochord. *Cell* **76**, 761-775. doi:10.1016/0092-8674(94)90514-2

Saint-Germain, N., Lee, Y. H., Zhang, Y., Sargent, T. D. and Saint-Jeannet, J. P. (2004). Specification of the otic placode depends on Sox9 function in *Xenopus*. *Development* **131**, 1755-1763. doi:10.1242/dev.01066

Saint-Jeannet, J.-P. and Moody, S. A. (2014). Establishing the pre-placodal region and breaking it into placodes with distinct identities. *Dev. Biol.* **389**, 13-27. doi:10.1016/j.ydbio.2014.02.011

Sasai, Y., Lu, B., Steinbeisser, H., Geissert, D., Gont, L. K. and De Robertis, E. M. (1994). Xenopus chordin: a novel dorsalizing factor activated by organizer-specific homeobox genes. *Cell* **79**, 779-790. doi:10.1016/0092-8674(94)90068-X

Sater, A. K. and Moody, S. A. (2017). Using *Xenopus* to understand human disease and developmental disorders. *Genesis* **55**. doi:10.1002/dvg.22997

Schlosser, G. (2006). Induction and specification of cranial placodes. *Dev. Biol.* **294**, 303-351. doi:10.1016/j.ydbio.2006.03.009

Segerdell, E., Ponferrada, V. G., James-Zorn, C., Burns, K. A., Fortriede, J. D., Dahdul, W. M., Vize, P. D. and Zorn, A. M. (2013). Enhanced XAO: the ontology of *Xenopus* anatomy and development underpins more accurate annotation of gene expression and queries on Xenbase. *J. Biomed. Semantics* **4**, 31. doi:10.1186/2041-1480-4-31

Shang, N., Lee, J. T. Y., Huang, T., Wang, C., Lee, T. L., Mok, S. C., Zhao, H. and Chan, W. Y. (2020). Disabled-2: a positive regulator of the early differentiation of myoblasts. *Cell Tissue Res.* **381**, 493-508. doi:10.1007/s00441-020-03237-2

Sive, H. L., Grainger, R. M. and Harland, R. M. (2007a). Removing the vitelline membrane from *Xenopus laevis* embryos. *CSH Protoc* **2007**, pdb prot4732. doi:10.1101/pdb.prot4732

Sive, H. L., Grainger, R. M. and Harland, R. M. (2007b). *Xenopus laevis in vitro* fertilization and natural mating methods. *CSH Protoc* **2007**, pdb prot4737. doi:10.1101/pdb.prot4737

Slater, L. T., Gkoutos, G. V. and Hoehndorf, R. (2020). Towards semantic interoperability: finding and repairing hidden contradictions in biomedical ontologies. *BMC Med. Inform. Decis. Mak.* **20**, 311. doi:10.1186/s12911-020-01336-2

Song, R., Walentek, P., Sponer, N., Klimke, A., Lee, J. S., Dixon, G., Harland, R., Wan, Y., Lishko, P., Lize, M. et al. (2014). miR-34/449 miRNAs are required for motile ciliogenesis by repressing cp110. *Nature* **510**, 115-120. doi:10.1038/nature13413

Spokony, R. F., Aoki, Y., Saint-Germain, N., Magner-Fink, E. and Saint-Jeannet, J. P. (2002). The transcription factor Sox9 is required for cranial neural crest development in *Xenopus*. *Development* **129**, 421-432. doi:10.1242/dev.129.2.421

Square, T., Jandzik, D., Cattell, M., Coe, A., Doherty, J. and Medeiros, D. M. (2015). A gene expression map of the larval *Xenopus laevis* head reveals developmental changes underlying the evolution of new skeletal elements. *Dev. Biol.* **397**, 293-304. doi:10.1016/j.ydbio.2014.10.016

Stennard, F., Carnac, G. and Gurdon, J. B. (1996). The *Xenopus* T-box gene, Antipodean, encodes a vegetally localised maternal mRNA and can trigger mesoderm formation. *Development* **122**, 4179-4188. doi:10.1242/dev.122.12.4179

DEVELOPMENT

Tapley, B., Michaels, C. J. and Doherty-Bone, T. M. (2015). The tadpole of the Lake Oku clawed frog *Xenopus longipes* (Anura; Pipidae). *Zootaxa* **3981**, 597-600. doi:10.11646/zootaxa.3981.4.10

Tasca, A., Helmstadter, M., Brislinger, M. M., Haas, M., Mitchell, B. and Walentek, P. (2021). Notch signaling induces either apoptosis or cell fate change in multiciliated cells during mucociliary tissue remodeling. *Dev. Cell* **56**, 525-539.e6. doi:10.1016/j.devcel.2020.12.005

Van Slyke, C. E., Bradford, Y. M., Westerfield, M. and Haendel, M. A. (2014). The zebrafish anatomy and stage ontologies: representing the anatomy and development of Danio rerio. *J. Biomed. Semantics* **5**, 12. doi:10.1186/2041-1480-5-12

Vize, P. D., Jones, E. A. and Pfister, R. (1995). Development of the Xenopus pronephric system. *Dev. Biol.* **171**, 531-540. doi:10.1006/dbio.1995.1302

Vokes, S. A. and Krieg, P. A. (2002). Endoderm is required for vascular endothelial tube formation, but not for angioblast specification. *Development* **129**, 775-785. doi:10.1242/dev.129.3.775

Walentek, P., Beyer, T., Thumberger, T., Schweickert, A. and Blum, M. (2012). ATP4a is required for Wnt-dependent Foxj1 expression and leftward flow in Xenopus left-right development. *Cell Rep* **1**, 516-527. doi:10.1016/j.celrep.2012.03.005

Wyatt, B. H., Amin, N. M., Bagley, K., Wcisel, D. J., Dush, M. K., Yoder, J. A. and Nascone-Yoder, N. M. (2021a). Single-minded 2 is required for left-right asymmetric stomach morphogenesis. *Development* **148**, dev199265. doi:10.1242/dev.199265

Wyatt, B. H., Raymond, T. O., Lansdon, L. A., Darbro, B. W., Murray, J. C., Manak, J. R. and Dickinson, A. J. G. (2021b). Using an aquatic model, *Xenopus laevis*, to uncover the role of chromodomain 1 in craniofacial disorders. *Genesis* **59**, e23394. doi:10.1002/dvg.23394

Xu, Y., Park, S. J. and Gye, M. C. (2019). Effects of nonylphenols on embryonic development and metamorphosis of *Xenopus laevis*: FETAX and amphibian metamorphosis toxicity test (OECD TG231). *Environ. Res.* **174**, 14-23. doi:10.1016/j.envres.2019.04.010

Zahn, N., Levin, M. and Adams, D. S. (2017). The Zahn drawings: new illustrations of *Xenopus* embryo and tadpole stages for studies of craniofacial development. *Development* **144**, 2708-2713. doi:10.1242/dev.151308

Zhou, X. and Vize, P. D. (2004). Proximo-distal specialization of epithelial transport processes within the *Xenopus* pronephric kidney tubules. *Dev. Biol.* **271**, 322-338. doi:10.1016/j.ydbio.2004.03.036

Zorn, A. M. and Mason, J. (2001). Gene expression in the embryonic *Xenopus* liver. *Mech. Dev.* **103**, 153-157. doi:10.1016/S0925-4773(01)00341-0

Figure S1

KEY

☐ Illustration not available
☑ Illustration available
☑ (light grey) Zahn Illustration available as line drawings
☑ (dark grey) Zahn illustration from XenHead project
n/a not applicable

Fig. S1. A comparison of available illustrations of *Xenopus laevis* developmental stages from Nieuwkoop and Faber's Normal Table (1994 edition) and those by Natalya Zahn. Check boxes show drawings which illustrate each stage in the view indicated in column headers (i.e., animal vegetal/ventral, vegetal-posterior, anterior, ventral dorsal, lateral). Note that Nieuwkoop and Faber's NF stage 3 and NF stage 4 'dorso-lateral' views are recorded in the 'lateral' view column, and NF stage 13, 14 15 and 16 'post-dorsal' views are recoded here in the 'dorsal' view column. Light grey shaded cells indicate that line drawings (n= 56) are available for specified stage/view. Darkly shaded cells indicated drawings are the those commissioned from XenHead project (Zahn et al., 2017). Open box: drawing not available. n/a: not applicable. Total Nieuwkoop and Faber illustrations = 125, and total Zahn illustrations = 142 (plus an additional 56 simple line illustrations), when counting each limb bud as an individual drawing in both series. Many of the Zahn drawings (but not all) are available as both complex, fully shaded illustrations and as simple unshaded line drawings. All drawings are available on Xenbase, but note that only the Zahn drawings are open access, and can be reused using this citation: Illustration © 2021 Natalya Zahn, CC BY-NC 4.0.
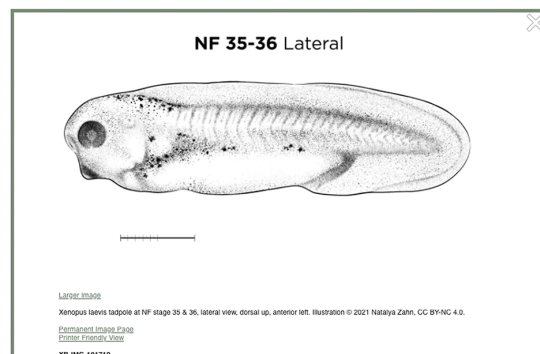
Figure S2

A

B

C

Fig. S2. Xenbase XAO pages for *Xenopus* embryo stages. Each XAO page for embryonic stages on Xenbase has a definition, based on the Nieuwkoop and Faber Normal Table, and is populated with Zahn drawings and other images (e.g., photographs from stereomicroscopy) when available. A. XAO page for NF stage 28. B. XAO page for NF stage 35 & 36, illustrated with a *Xenopus* community submitted image taken by Matthew Kofron (used here with their kind permission). C. Pop-up window from NF stage 35 & 36, activated by double click on the image, shows a larger view and has a left-right scroll arrow to view all images posted to this page, including Zahn drawings. Links from the pop-up will enlarge an image further or give researchers a printer friendly view.

Figure S3

A

B

Fig. S3. Xenbase XAO anatomy terms pages. Anatomical entities (i.e., primary germ layers, cell types, tissues, organs, structures) are individual terms in the *Xenopus* anatomy ontology, the XAO. XAO terms used in the Landmarks Table link to the specific XAO page where information about that term is collated. A. XAO page (Summary tab) for heart (XAO:0000064), where the definition is based on Nieuwkoop and Faber's (1956) Normal Table criteria, and a curated list of molecular markers from Xenbase gene expression data are given. B. Expression tab of XAO page for heart collates all curated gene expression data. Columns are sortable based on number of primary sources, predominantly images (curated gene expression data from published research articles) and papers (where gene and anatomy are co-referenced). Click 'Images' heading to sort genes with the most curated gene expression figures from primary sources (and therefore the best candidates for molecular markers) at the top of the list.

Table S1. *Xenopus laevis* staging landmarks. For a live online Xenbase version see:
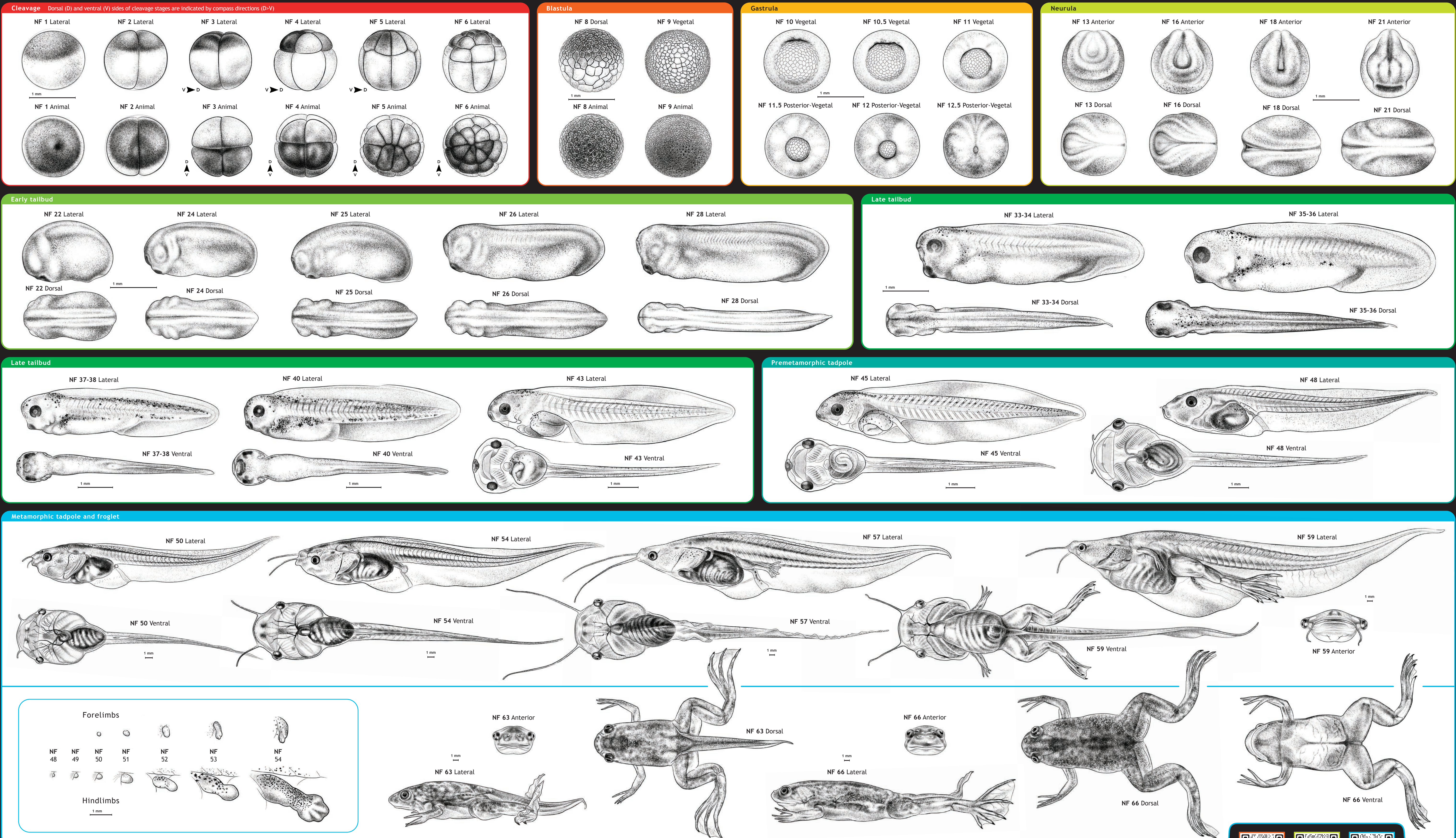
https://www.xenbase.org/entry/landmarks-table.do

Developmental Process	NF stage number	NF stage name	LANDMARKS		
			EXTERNAL	INTERNAL	MOLECULAR MARKERS [*gene: anatomy*]
FERTILIZATION	n/a	mature egg	1 cell; ovulated unfertilized egg; animal hemisphere dark, vegetal hemisphere light; animal-vegetal axis in random orientation; soft texture	large nucleus, 'germinal vesicle' in animal hemisphere	*nanos1: mitochondrial cloud; vegt: vegetal cortex*
FERTILIZATION	1	1-cell, fertilized egg	1 cell; vitelline membrane swells; eggs rotate with dark animal hemisphere up, light vegetal hemisphere down; firm texture; sperm entry point indictated by pigment condensation; germinal vesicle breakdown leaving pale spot in animal hemisphere	cleavage has not begun; germinal vesicle breaks down and pronuclei fuse; visible cortical layer thickest on animal and dorsal sides.	
CLEAVAGE	2-		first cleavage begins as a top to down furrow in animal hemisphere	cleavage furrow has not yet reached the vegetal pole	
CLEAVAGE	2	2-cell	2 cells; 1st cleavage plane is meridional along the dorso-ventral plane dividing right and left halfs		*sox3, atp4a: animal hemisphere; vegt: vegetal hemisphere*
CLEAVAGE	3	4-cell	4 cells; 2nd cleavage is meridional, perpendicular to the 1st cleavage; in many embryos, the 2 dorsal blastomeres (left and right) are smaller and lighter (on animal surface) than 2 larger darker ventral blastomeres (also left and right)[1]	cleavage cavity present	
CLEAVAGE	4	8-cell	8 cells; 3rd cleavage plane is equatorial giving 4 smaller animal blastomeres (micromeres) and 4 larger vegetal blastomeres (macromeres); animal dorsal cells are lighter and ventral cells are darker in some embryos	center	*nanos1: germ plasm; hwa: dorsal Wnt signalling*
CLEAVAGE	5	16-cell	16 cells; 4th cleavage is again meridional; animal blastomeres smaller than vegetal blastomeres; dorsal blastomeres lighter than ventral.		
CLEAVAGE	6	32-cell	32 cells; 5th cleavage equatorial, giving 4 rows each with 8 blastomeres; animal pole with smallest rosette of micromeres, 2 middle rows of irregular shaped cels, larger vegetal rosette of macromeres		
CLEAVAGE	6.5	morula	64 cells; 6th cleavage; cleavages becomming asynchronous; animal/dorsal blastomeres divide before vegetal blastomeres		*gdf1: vegetal hemisphere; shroom1, tfap2a: animal hemisphere*
BLASTULA	7	early blastula	128-512 cells; 7th-9th cleavages, no longer possible to count cells reliably; size of animal cells used to distinguish embryo stage	clear delineation of the 3 primary germ layer tissues; notochord begins to form from mediolateral convergence of dorsal presumptive axial mesoderm under the neural ectoderm	*nodal5 (nr5): earliest zygotic transcription*
BLASTULA	8	middle blastula	~1000-4000 cells; 10-12+ cleavages; cell number no longer a stage guide; animal hemisphere with small dark pigmented cells refered to as 'animal cap'; animal surface looks 'pebbly'	at NF stage 8.5, after 12th cell divisions the mid-blastula transition (MBT) occurs; asynchronous internal cell division; zygotic genome activation	*gs17, nr1: major initiation of zygotic transcription*
BLASTULA	9	late blastula	animal hemisphere still darkly pigmented; animal surface more like 'grains of sand' than 'pebbles' of NF stage 8	blastocoel now maximum size; 3 germ layers becoming distinct; ectoderm in the animal 1/3 of the embryo, a ring of mesoderm in the middle and yolky endoderm on the vegetal 1/3	*sox17a: endoderm; tbxt: mesoderm*
GASTRULATION	10	initial gastrula	darker pigment from bottle cells on the dorsal vegetal surface indicate dorsal blastopore lip formation, between '11 & 1 o'clock'; blastopore groove where cell ingress, is not yet visible	initial formation of Spemann Organizer at the dorsal marginal zone/upper blaspore lip	*gsc: upper blastopore lip; tbxt: marginal zone*
GASTRULATION	10.25	early gastrula	blastopore lip extends laterally ~1/4 around the circumference, from ~ '10 to 2 o'clock' ; indentation of blastopore visible as a groove	marginal zone involutes on dorsal side; internally, dorsal endomesoderm begins to migrate anteriorly along bastocoel surface; vegetal rotation of endoderm mass	
GASTRULATION	10.5	crescent-shaped blastopore	arch of pigmented blastopore lip extends laterally from doral to lateral sides ~1/4 to 1/2 around the circumference; yolk plug almost round	medial-lateral intercalation of dorsal mesoderm; 'Brachet's cleft' forms between internal leading edge endomesoderm and the dorsal mesoderm; neural induction begins, dorsal-ventral patterning	*chrd.1, lhx1: involuted dorsal mesoderm; ventx2.1, wnt8a: ventro-lateral marginal zone; hhex: anterior endomesoderm*
GASTRULATION	11	horse-shoe shaped blastopore	pigmented blastopore lip ~ half the circumference, pigmented bottle cells extend to the ventral side; yolk plug ~1/2 diameter of embryo, is slightly elongated in the dorsal-ventral direction	Brachet's cleft begins to open forming the archenteron; ectoderm, mesoderm and endoderm germ layers specified; blastocoel becoming smaller, mesodermal mantle undergoes convergent extension and endoderm is internalized	*sox17a: endoderm; tbxt: mesoderm; sox2: neurectoderm; krt12.4: non-neural ectoderm*
GASTRULATION	11.5	large yolk plug	blastopore lip extends all the way around yolk plug; lower/ventral blastopore lip more darkly pigmented; yolk plug not quite round, ~1/3 of embryo diameter elongated in the dorsal-ventral direction	blastocoel displaced to the ventral side; involuting 'endomesoderm' mantle continues to extent anteriorly	
GASTRULATION	12	medium yolk plug	areas of light and dark pigment radiating from yolk plug (flower petal like); yolk plug small and circular, a little less than 1/4 of egg diameter, diameter decreasing; neurectoderm transforming into the discernible neural plate	blastocoel begining to close as the archenteron expands	*sox2, sox3: neural plate*
GASTRULATION	12.5	small yolk plug	darker pigment lines on dorsal surface indicate future neural groove and neural plate; blastopore slit is slightly open, diameter decreasing and oval shaped	clear delineation of the 3 primary germ layer tissues; notochord forms from mediolateral convergence of dorsal axial mesoderm under the neural ectoderm	*chrd.1, nog, shh: axial mesoderm, notochord*
GASTRULATION	13	slit blastopore	blastopore completely closed to a 'slit'; neural plate on dorsal side clearly outlined	neural crest form at the neural plate border, i.e., the boundary between the neural and non-neural ectoderm	*sox2, sox3: neural plate; ednra, msx1: neural plate border; snai2: neural crest; tbx2: cement gland primordium; myf5: paraxial medoderm; rax: optic field*
NEURULATION	13.5	initial neural plate	sharp demarcation of anterior neural plate; anterior aspect of neural plate bent down; yolk plug internalized		*tubb2b: differentiating neural progenitors; msx1: anterior neural plate border*
NEURULATION	14	neural plate	neural plate obvious; dorsal midline thin with neural folds thickening anteriorly and laterally; neural folds begin to elevate; convergence extension begins to narrow neural plate posteriorly	blastocoel continues to close in the ventral foregut region as archenteron expands on the internal dorsal side	*pax6: optic field, neural plate, lens placode; pax2: between anterior and posterior neural plate*
NEURULATION	15	early neural fold	neural folds distinct; anterior neural fold round; demarcation of neural plate clear caudally, narrowing in middle and caudal regions; neural groove deepens; pigmented cement gland primordium faintly visible at the ventral-anterior border of neural plate, cells stand out from epithelial layer.	physical segregation of cranial neural crest from anterior (pre-chordal) neural plate; blastocoel closes in the ventral foregut	*pax3: neural fold/neural crest; pax8: intermediate mesoderm; rax, otx2, six3: optic field; hhex: foregut endoderm*
NEURULATION	16	mid-neural fold	eye primordia [2] become discernable as indentations near the lateral edges of the anterior neural plate; anterior neural plate 'rectangular' in shape; neural plate sharply constricted in the middle.	right and left cardiac mesoderm migrates to anterior-ventral midline; foregut diverticulum forms	*pax6: optic field, anterior neural plate, and lens placode; nkx2-5: cardiac progenitors; krt12.4: ectoderm, non-neural ectoderm, epidermis*
NEURULATION	17	late neural fold	anterior neural plate oblong, triangular, angles formed by eye primordia [2]; clear neurentic canal along midline, posterior end of which continues over closed blastopore slit; neural folds closing in trunk region	delineation of cranial neural crest lateral to the anterior neural plate; 1st indication of somite segregation from presomitic mesoderm	*sox2, sox3: neural plate/neurenteric canal; otx2, rax, pax6, six1, sox2: optic field; lhx1: intermediate mesoderm*
NEURULATION	18	neural groove	anterior part of neural plate narrow, club shaped; parallel neural folds very close but not touching	neural crest segregation begins; 3-4 anterior somites segregate from paraxial mesoderm	*myod1: early somites and presomitic mesoderm; casz: early somites; snai1, egr2, twist1: neural crest; pax8: otic placode.*
NEURULATION	19	initial neural tube	neural folds mostly closed forming a neural tube, except for an open slit in the anterior neural plate; neurenteric canal deepening; dark pigmented cement gland primordium immediately ventral to anterior neural plate; laterla view of embryo convex oval, not elongated	migration of 4 neural crest streams begins; 4-6 anterior somites segregated	*ag1, agr2: cement gland primordium*
NEURULATION	20	fused neural tube	neural tube fused anteriorly; no pharyngeal bulge visible; dark oval cement gland primordium below border of anterior neural plate; embryo starts to elongate; optic cup (eye primordium) forms; oral evagination (mouth) visible	neural crest extends to front to eye; paired glomus primordia present [2] ; anterior 6-7 somites; thickening of cardiac mesoderm	*rax, pax6, otx2, six3: optic vesicle; wt1, rgn: glomus; nkx2-5: cardiac progenitor cells; egr2: rhombomeres R3, R5, and neural crest; en2: midbrain-hindbrain boundary; snai2: neural crest; chrd.1, nog, ssh: notochord*
NEURULATION	21	neural tube	embryo has a dorsal curvature, with flat ventral surface; one pharyngeal arch bulge; neural tube completely closed; optic vesicle ('eyes') begin protuding, forming 2 oblique 'oval spots'; multiciliated cells form on the surface of the epidermis	8-9 somites; first indication of pronephric mesenchyme; otic placodes form posterior to optic vesicle	*pax6, lim1: pronephric mesenchyme; nrp1: neural tube; pax3: hatching gland; tuba4b, cfap206, foxj1: multiciliated epidermal cell*

Stage		Name	EXTERNAL	INTERNAL	BEHAVIOR & PHYSIOLOGY	MOLECULAR MARKERS
EARLY ORGANOGENESIS	22	early tailbud	embryo begins to elongate (convergent extension); ventral surface slightly concaved; two pharyngeal arch bulges; distinct eye protrusion; anal opening displaced to ventral side	9-10 somites; ventral blood island forms; segreation of forebrain, midbrain and hindbrain		***gsx1, sox3:*** brain segments; ***gata1, hba3, tal1:*** ventral blood island; ***nodal1:*** lateral plate mesoderm on the left side only; ***tbx6, foxd4l1.1:*** early tail bud
	23	early tailbud	ventral surface concave giving embryo a 'coffee bean' look; two pharyngeal arch bulges; olfactory placodes thicken between eyes; slight depression of otic placode; jaw and gills separated by groove; "inverted Y shaped" hatching gland between eyes to cement gland	12 somites; forebrain regions telencephalon and diencephalon distinguishable		***cxcl14, astl3a.1, pax3:*** hatching gland; ***myod1:*** somites and presomitic mesoderm; ***six1:*** olfactory placode; ***pax2, pax6, vax2:*** diencephalon; ***foxg1:*** telencephalon
	24	early tailbud	noticable elongation of the embryo and tail bud outgrowth; in dorsal view, eyes protruding out laterally less than gills; gill primordium area smooth (ungrooved)	15 somites; primary germ cells detecable in cell trunk endoderm; primary and secondary heart fields indictated in heart primordium	initial motor reactions to external stimuli	***tbxt, lmo2, aplnr:*** tail bud; ***tnni3, nkx2-5:*** primary heart field; ***bmp4:*** secondary heart field; ***grip2, pgat:*** primordial germ cells; ***pcdh8.2:*** otic vesicle and tail bud; ***eya2:*** otic vesicle
	25	early tailbud	embryo still convex dorsally and concave ventrally; eyes protruding out laterally equal to or more than gills, gills now grooved; otic vesicle pigmented	16 somites; head somite 1 diminished; brain flexure ~90o	multi-cilliated cells in the epidermis become active	***ag1:*** cement gland; ***tubb2b:*** brain and spinal cord
	26	tailbud	If liberated from the vitelline membrane the embryo is straight, not convex dorsally; if the embryo remains in the vitelline membrane it is curved laterally; tail bud obvious; otic (ear) vesicle protruding	17 somites; head somite I disintegrated; pronephros distinct; myotomes distinct	spontaneous movements begin	***pax8, hnf1b, irx3:*** pronephric mesenchyme
	27	tailbud	tail bud defined in lateral view; fin translucent; lens begins to form, eyes flatten laterally; otic vesicle closes	heart fields merge forming a triangular-shape at ventral midline, behind the cement gland primordium and anterior to liver diverticulum; 19 somites		***pax6, sox3, prox1, foxe3, nrl:*** lens; ***neurod1, sox3:*** epibranchial placodes
ORGANOGENESIS	28	tailbud	tail bud elongates distally and extends downward to cloaca; fin divided into outer transparent (outer fin) and inner translucent bands (inner fin); black cement gland fully formed; otic vesicle separates from epidermis	heart primordium and pericardial cavity discernible; pronephric nephrostomes form; 20-22 somites; epibranchial placodes first segregate	embryos liberated from the vitelline membrane glide around due to multi-cilliated cell fluid flow	***hand2, actc1:*** endocardial tube; ***dlx2, sox9, sox10:*** cranial neural crest; ***pax5, lhx1:*** nephrostomes; ***neurog2, eya1:*** epibranchial placodes; ***fgf8, sox9:*** otic vesicle
	29 & 30	late tailbud	tail bud distinct; outer fin edge transparent over entire length; gray disc of the eye cup now visible	23-25 somites segregated to end of tail; lumen in pronephric kidney collecting duct; appearance of glomus and thyroid; neural tube closure has formed the spinal cord		***runx1:*** olfactory placode; ***lhx9:*** brain segments; ***foxa2, tubb2b:*** spinal cord; ***nphs1, wt1:*** glomus; ***nkx2-1:*** thyroid primordium; ***not:*** tail tip
	31	late tailbud	tail bud equal in length and height; nasal/olfactory pits first indicated	heart primordium extends ventrally and bends slightly to right; 22-23 post-otic somites; midbrain-hindbrain boundary distinct		***hey1, myod1, actc1:*** somites; ***en2, pax2, fgf8:*** midbrain-hindbrain boundary
	32	late tailbud	tail bud ~1.5x longer than height; eye cup distinct, U-shaped (open); mouth primordium not visible	heart a linear tube with anterior outflow tract, left ventricle, atrioventricular canal and atrium; 26 post-otic somites; pronephric nephrostomes form; lung buds visible		***pax2, vax1:*** optic stalk; ***cfap161:*** nephrostomes and multicilliated epidermal cells; ***nkx2-1:*** lung and thyroid progenitors; ***aldh1a3, agr2:*** otic vesicle
	33 & 34	late tailbud	tail bud ~2x longer than height; gut ~3 x longer than tail; eye cup open C-shape with darker pigmentation dorsally; mouth primordium a shallow vertical groove; 32 post-otic somites; pigmented cells (melanophores) first appear on head (near hindbrain) and anterior trunk (near pronephric kidney)	heart looping begins; heart beat clearly observable; foregut begin to constrict at trachea-ephagus boundary; cranial nerves distinct; thyroid primordium discernible [2]; pronephric kidney and duct formed with surrounding vasculature; thyroid primordium detectable		***dab2:*** pronephric sinus, posterior cardinal vein; ***sox2:*** dorsal foregut; ***tubb2b:*** cranial nerves; ***myl2, bves:*** heart; ***actc1, mybpc3:*** heart and somites; ***pax2, lhx1:*** pronephric kidney and pronephric nephrostomes [2]
	35 & 36	free swimming tadpole [3]	tail bud ~3x longer than height; gut ~2 x longer than tail; outline of the proctodeum still curved; optic vesicle/retina completely black; choroidal fissure open; cardiac mesoderm starts to spontaneously contract; mouth invagination not quite round; 2 gill lobes; 36 post-otic somites; melanophores extend over top of head and along dorsal trunk	heart S-shaped, with distinct atrium lying dorsal to ventricle; vasculature to head and tail developing; liver bud visible posterior to heart; pronephric duct fused with rectal diverticulum, pronephric nephrostomes obvious	embryos naturally hatch from vitelline membrane to become free swimming	***aplnr, hbz:*** blood vessels and heart; ***onecut, nrlh5, hhex:*** liver; ***aldh1a1:*** pronephric kidney/duct, choroidal fissure and olfactory bulb; ***tal1, hba3:*** ventral blood island; ***nkx3.2:*** mouth primordium
	37 & 38	free swimming tadpole	gut almost same length as tail; eye's choroid fissure closing ventrally but remain open; mouth invagination deep, round-shaped; heart contractions obvious, blood flow visible; proctodeum at obtuse angle (~140 degrees) to tail somites; 40 post-otic somites; melanophores extend over tail	paired lymph hearts; entire pronephric kidney functioning; ventral bud of pancreas formed;		***tnni3:*** heart; ***sftpc:*** lung buds; ***myh6:*** lymph heart; ***atp1a1:*** pronephric kidney and pronephric duct; ***nkx2-1:*** thyroid and lungs; ***foxe3:*** thyroid and lens; ***ptf1a, pdia2:*** pancreatic buds
	39	free swimming tadpole	gut equal in length to tail somites; melanophores around nasal pits & along ventral edge of tail somites; ventral choroid fissure nearly closed; proctodeum at ~125 degree angle to tail somites; 43 post-otic somites	retinal ganglion cell axons reach optic tectum; mesonephric kidney forms		***bmp4, hoxa13:*** proctodeum; ***map2, pou4f1:*** retinal ganglion cell layer; ***insm1, nos1:*** optic tectum
GUT-COILING	40	free swimming tadpole	tail now longer than the abdomin; optic choroid fissure completely closed; mouth opening 'breaks through'; stomach and pancreas visible on the left side of gut; proctodeum at 90 degree angle to tail somites (lateral view), ~45 post-otic somites	gall bladder primordium formed and sometimes visible (irridescent on ventral view); blood circulation in gills visible	embryos begin taking gulps of air from the surface	***cela1.2:*** pancreas; ***sfrp5, klf5:*** stomach; ***onecut, hhex, sox17a:*** gall bladder; ***hhex, nr1h5:*** liver
	41	free swimming tadpole	conical shaped proctodeum formed, at angle of ~ 60 degrees to tail somites	myocardium thickens and develops trabeculae, atrium posterior to ventricle; torsion of gut starts; post-anal gut disappears; the pancreas, now visible in ventral view, posterior to left-sided stomach		***clcnkb:*** pronephros; ***ins:*** pancreas; ***myod1:*** tail somites; ***sfprf:*** brain segments; ***nkx2-5, tpm1:*** myocardium; ***hoxa13:*** proctodeum
	42	free swimming tadpole	opercular fold first visible; head somites I and II disappeared	trachea and esophagus seperate		***sox2:*** esophagus and stomach; ***nkx2.1:*** trachea and lung buds; ***sftpc:*** lung buds
	43	free swimming tadpole	cement gland starts to lose pigmentation; lateral line pits visible	stomach has lengthened further; pancreas shifted to right side [5]; duodenum formed by 1st gut coil constriction to anterior-right; midgut and hindgut form hairpin curve, visible on left side (will become the 'apex' of future intestinal coil)		***foxg1, spdef, bmpr1a, cfap161:*** stomach; ***cela1.2:*** pancreas; ***aldh1a2:*** duodenum;
	44	free swimming tadpole	heart fully formed and clearly visible; barbels/tentacles start to grow; gills/branchial basket shrinking	septum begins to form in cardiac atrium which is slightly anterior to ventricle; midgut and hindgut lengthened more; the intestinal apex visible in ventral view as a "U" shape in the upper left quadrant of the gut cavity	visual avoidance behavior begins	***tnni3, frzb, sox9, nkx2-5:*** heart; ***cdx2:*** midgut-hindgut
	45	feeding tadpole [3]	operculum partly covers the gills; hindlimb bud not visible	midgut and hindgut continue to lengthen; the intestinal apex begins to rotate inward in a counterclockwise trajectory; spleen forms; mesonephric kidney	tadpoles to start swim continuously and begin feeding	***darmin, a2m:*** midgut, hindgut and liver; ***nkx2-5:*** spleen primordium
PREMETAMORPHOSIS	46	feeding tadpole	crescent-shaped hindlimb bud first appears although is difficult to see; pigment cells appear on eye and around abdomen; trunk somite 1 disappeared	midgut and hindgut lengthen further- apex continues to rotate inward, forming multiple coils of intestine; blood circulation to gills diminishing	food can be seen in intestine as now feeding	
	47	feeding tadpole	irredescent gold-coloured abdominal wall surrounds coiled gut; blood circulation visible from heart to gills, and through paired dorsal aorta; cement gland starts to degenerate; barbels/tentacles longer	retinal ganglion cells have formed complex synapses with optic tectum neurons; thyroid gland begins to function; thymus gland detectable		***foxn1:*** thymus
	48		hindlimb bud now clearly visible, with nearly semi-circular shape	retinal ganglion cells-optic tectum synapses more compact		***fgf8, spry1, sall4:*** hindlimb bud
	49		hindlimb bud length equal to it's width	thyroid follicles first appear		
	50		hindlimb bud slightly constricted at base; tiny oval forelimb buds just visible	gonads undifferentiated		***hoxa13:*** forelimb bud; ***spry4:*** hindlimb bud
	51		hindlimb bud is cone-shaped; forelimb bud is oval shaped (in lateral view)	resorption vacuoles in thyroid follicles first appear		***hoxd10, hoxa13, hoxa9:*** hindlimb bud
	52		hindlimb bud with slight 'wrist' indent; forelimb bud slightly constricted at base	5 complete coils of the intestine (internal and external coils)	regeneration competent [4]	***sox9:*** hindlimb digits (cartilage elements)

	Stage	Name	Morphology	Organs	Notes
PROMETAMORPHOSIS	53		hindlimb bud paddle-like, with wrist constriction, hindlimb digits not discernable; forelimb bud with slight wrist constriction	onset of sexual differentiation of gonads	regeneration competent; athyroid animals have arrested development
	54		hindlimb bud length (not including foot) 2x the width; foot paddle splayed with 5 digits and thinner inter-digital webbing; forelimb paddle with 4 digits and thinner inter-digital membranes	pronephric kidney begins to atrophy	thyroid hormone detectable in blood *tbx4, sall4*: interdigital mesenchyme
	55		hindlimb length (not including foot) 3x width; forelimb hand rotates 90 degress, free parts of fingers as long as they are wide	all major muscles of hindlimb developed	regeneration restricted [4]
	56		hindlimbs visible from above as they can rotate away from body; hindlimb length = ~ 5 tail somites; larval pigmentation pattern established	sexual differentiation of gonads into ovary or testis; hindlimb skeleton completey chondrified	regeneration restricted [4]
	57		hindlimb length = ~ 9 tail somites; forelimb remains enclosed in operculum; lip folds form		
	58		hindlimb length = 11-12 tail somites; claws form on toes 1-3 (mostly always still white); forelimb emerges from operculum, elbows first; tail tip begins to atrophy	melanin/pigment deposited in under skin especially in tail	regeneration incompetent [4]
	59		hindlimb muscular, claws start to harden and turn black, shortest toes first; finger tips reach base of hindlimb when forelimb is positioned along the abdomen; tentacles/barbels regress	melanin/pigment surrounds intersomitic blood vessels and between fibres of somites; forelimb muscles differentiated; pronephros no longer functional	regeneration incompetent [4]
	60		gill chamber opening still wide; fingertips reach beyond base of hindlimb (almost to 'knee') when forelimb/arm is positioned along side of the abdomen; forelimb held posterior to heart; tail fins greatly reduced	pigmentation across body increases	regeneration incompetent [4]; animal switches from tail to leg swimming
	61		first sign of gill resorption, openings to gill chamber much narrower; hindlimb and forelimb fully formed; forelimb at level of posterior half of heart	lateral finger-like protrusions from olfactory organ	cessation of feeding (due to oral and intestinal remodeling) *obp*: olfactory organ
CLIMAX OF METAMORPHOSIS	62	tailed froglet	head slightly broader than abdomen; corner of mouth still infront of eye; forelimb reaches middle of heart; ventral tail fin gone from abdomen; adult skin on hindlimbs; only tiny nubs of barbels/tentacles remain.	tiny 'stirnorgan' (light detecting cells/part of pineal gland) appears; notochord atrophies along length of tail	peak levels of thyroid hormone in plasma
	63	tailed froglet	head narrower than abdomen; barbels/tentacles (most often) completely gone; forelimb at level of anterior half of heart; tail shortens as tail somites are rapidly resorbed, tail still slightly longer than body		
	64		corner of mouth behind eye; tail length is about 1/3 of body length, at level of ankle when legs are in typical neutral position; body completely covered in adult skin, but 'border lines' clearly visible	thymus gland ventral-lateral to otic capsule	
	65		tail length a few millimeters, all tail somites have disappeared; body completely covered in adult skin, but 'border lines' still visible in some areas		feeding resumes
	66	froglet	tail very nearly gone, not visible from ventral view; adult skin 'border lines' have disappeared, froglet body ~ 10mm long	skin remodelled with underlying dermis and secretory glands	thyroid hormone in plasma returns to prometamorphic levels

FOOT NOTES

1. Dorsal-ventral pigment variation only occurs in some batches of embryos. Select 2-4-cell embryos with clear pigment variation - otherwise only accurate about 70% of time.
2. In the Normal Table and other texts, organ primordia are often called 'anlage'; they are visualized by a thickening of specific cells via histology or by molecular markers. Search specific XAO terms on Xenbase for more molecular markers
3. NF stages 41-66 are not referred to by specific 'stage names' by Nieuwkoop and Faber
4. Regeneration classes from Aztekin et al 2021 PMID:34105722.
5. Left and right sides refer to that of the tadpole/embryo, and not the viewer.

The Zahn drawings: a new graphical resource of the Normal Table of *Xenopus* development

Illustrations of embryonic development from fertilized egg, through cleavage, gastrulation, neurulation, tailbud growth, tadpole, metamorphosis and froglet stages.

Natalya Zahn, Christina James-Zorn, Virgilio G. Ponferrada, Dany S. Adams, Julia Grzymkowski, Daniel R. Buchholz, Nanette M. Nascone-Yoder, Marko Horb, Sally A. Moody, Peter D. Vize and Aaron M. Zorn